SETCOR
Conferences & Exhibitions

The Global Advanced Materials & Surfaces GAMS 2022 International Conference

June 15 to 17 2022

Conference Proceedings

DOI:
https://doi.org/10.26799/cp-gams-2022

Proceedings of the GAMS 2022 International Conference
Paris, France – June 15 – 17, 2022
DOI: https://doi.org/10.26799/cp-gams2022

Investigation of bi-layered ZnO-Ni photocatalyst powder produced by reactive magnetron sputtering technique

M. Lelis[1], S. Tuckute[1], E. Demikyte[1], D. Galalyte[1], R. Daugelavicius[2], S. Sakalauskaite[2]

[1] Centre for Hydrogen Energy Technologies, Lithuanian Energy Institute, Breslaujos str. 3, Kaunas, Lithuania, martynas.lelis@lei.lt

[2] Faculty of Natural Sciences, Vytautas Magnus University, Vileikos str. 8, Kaunas, Lithuania, rimantas.daugelavicius@vdu.lt

Abstract

The goal of the current study was to produce magnetic photocatalyst powder consisting of bi-layered ZnO-Ni particles for easy manipulation and collection during the repetitive photocatalytic water treatments. First, magnetron sputtering was used to cover NaCl grains by Ni underlayer and ZnO overlayer. Then the salt was washed off with distilled water. SEM, EDS and XRD analysis confirmed that obtained particles can be characterized as bi-layered open shells with nanocrystalline ZnO phase on one side and metallic Ni on the other side. In laboratory tests larger part of initial bi-layered powder were successfully recollected by magnets even after 10 consecutive usage cycles. Measurements of photocatalytic performance demonstrated relatively high activity and stability of bi-layered ZnO-Ni powder. Photocatalytic treatment of *S. Typhimurium* bacteria with ZnO-Ni powder and UV light in 1 hour reduced *S. Typhimurium* viability by more than 98 %, but similar treatment using visible light was not efficient.

Keywords: ZnO, photocatalysis, photocatalytic degradation, magnetic, bi-layered nanomaterials.

1. Introduction

To be suitable for practical applications photocatalysts must be efficient and convenient to use. Different synthesis methods produce photocatalyst material with different merits. Sol–gel, thermal decomposition, coprecipitation, hydrothermal and other chemical methods commonly produce large surface area nanocrystalline powder [1]. But most often these methods also have a common disadvantage – it is relatively difficult to form multi-component materials with well controlled structure. Also, the use of photocatalyst powder is a practical challenge, because it is difficult to separate (collect) the used-up powder from the treated solution and to re-use them without losing significant part of the fine powder particles [2], [3]. On the other hand, magnetron sputtering, laser beam evaporation, molecular beam epitaxy and other physical methods usually deposit films and benefit from more defined control of the photocatalyst structure. Wherefore they are more convenient way to form heterostructures [4]. Photocatalyst films produced by physical methods are practical to handle and can be easily re-used, but physical methods most often cannot provide such high surface area and product output as chemical alternatives.

To lessen the issue of powder handling, in current study we decided to apply magnetron sputtering in not typical way and to use it for the synthesis of fine magnetic photocatalyst powder. The design of magnetic powder particles combined two functional layers: i) photocatalyst material and ii) magnetic metal which would make them responsive to the magnetic field. More specifically, the main task of the present study, was to produce bi-layered ZnO-Ni photocatalyst particles, to investigated their photocatalytic efficiency and to test powder collection possibilities during the repetitive photocatalytic water treatments. ZnO was chosen as one of the most appealing photocatalyst materials. Thermodynamically the most stable ZnO phase (hexagonal wurtzite [5]) is chemically and thermally stable at normal and high energy radiation conditions. It has similar band-gap as TiO_2 (~3.26 eV) and with proper modifications arguably can reach comparable photocatalytic efficiency as TiO_2 [6], [7]. For practical applications ZnO can be more attractive than TiO_2 because it is cheaper and it is relatively easier to form [8]. We chose Ni for the magnetic metal layer, because Ni is one of the most important ferromagnetic elements and is known for good catalytic properties [9], [10].

DOI: https://doi.org/10.26799/cp-gams2022

2. Methodology

Bi-layered ZnO-Ni samples were synthesized using a modified PVD-75 physical vapour deposition system manufactured by Kurt J. Lesker company. The scheme of the bi-layered ZnO-Ni coating formation is presented at Fig. 1. At first magnetron sputtering was used to deposit Ni layer on NaCl grains in an argon gas environment. Then reactive magnetron sputtering was used to deposit ZnO layer on top of the pre-coated salt. Main parameters of ZnO and Ni layer formation are presented in Fig. 1, whereas more specific details of the used reactive magnetron sputtering process can be found at [11].

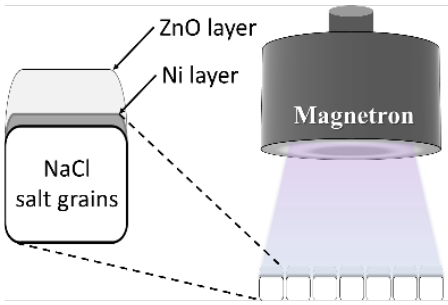

Main experimental parameters

Layer	Ni	ZnO
Target	Ni, Ø 76 mm, 99.99 %	Zn, Ø 76 mm, 99.99 %
Gas	Ar	Ar+O_2
Working pressure	1.3 Pa	1.0 Pa
Ar/O_2 flow ratio	-	≈ 3.4
Magnetron power	300 W (DC)	150 W (RF)
Layer thickness	up to 0.5 µm	up to 5.0 µm

Fig. 1: Experimental scheme and main parameters of the bi-layered ZnO-Ni coating formation.

After Ni and ZnO deposition, salt grains were dissolved and washed off by distilled water. The obtained bi-layered ZnO-Ni powder product was left to dry out for 48 hours at room temperature. Crystal structure of obtained ZnO-Ni powders was determined using X-ray diffractometer (XRD, Bruker D8). Morphological characteristics and elemental mapping of the powders were measured by scanning electron microscope (SEM, Hitachi S-3400N) equipped with energy dispersive X-ray spectrometer (EDS, Bruker Quad 5040).

Photocatalytic activity of the produced bi-layered ZnO-Ni powder was evaluated by the photocatalytic degradation of methylene blue (MB) and Rhodamine-B (RhB) aqueous solution under UV-A (365 nm) and visible light (400-800 nm) irradiation, respectively. For UV activated photocatalysis tests ZnO-Ni powder were placed in 40 mm diameter quartz vessel with 10 ml of MB solution (10 mg/L). To limit water evaporation reaction vessel was covered up by a high transparency fused silica wafer. The intensity of UV light source (Thorlabs M365LP1-C5) at the surface of reaction solution was 23.5 mW/cm^2. The temperature of the solution was maintained at 22 °C. Prior to irradiation, dye solution with a test sample was magnetically stirred (700 rpm) in the dark for 30 min to establish a MB adsorption-desorption equilibrium. The duration of one photocatalytic treatment test was 3 hours. During the experiment, at every 30 minutes 0.5 ml samples were taken from the container and measured by UV-VIS spectrometer (Jasco V-650) to determine the remaining dye concentration. After each measurement, the solution was immediately returned back to the reaction container. The same powder was used for 10 consecutive test cycles. After each cycle the used bi-layered ZnO-Ni powder were collected by magnetic stirring bar, the degraded MB solution was removed and a fresh one was added to the container. The stability of photocatalytic efficiency of ZnO-Ni powder under visible light was tested using the same experimental set up, just UV light source was replaced by a wide spectrum LED lamp (Thorlabs SOLIS-3C) and MB solution was replaced by RhB (10 mg/L). After the dye bleaching tests, ZnO-Ni powder were also used for the photocatalytic disinfection of *S. Typhimurium* bacteria under UV and visible light irradiation following the procedure described at [11].

3. Results and Discussion

Fig. 2a and 2b show general and more detailed microstructure views of the as-deposited ZnO-Ni films, respectively. SEM images revealed that magnetron sputtering deposition process was capable to produce generally uniform continuous coatings which nicely repeated the curvature of the NaCl grains. Interestingly, the microstructure of the films on NaCl grains was very similar to the ZnO films which were earlier received on flat glassy substrates [12]. The EDS analysis of the washed off powder product (Fig. 2c-e) demonstrated that some powder faces were dominated by Zn and O elements, whereas others were composed of Ni. This indicated that bi-layered films were successfully produced. XRD analysis

DOI: https://doi.org/10.26799/cp-gams2022

was carried out to investigate the phase composition of the bi-layered powders. XRD data (Fig. 3) confirmed the presence of hexagonal wurtzite ZnO phase. The pattern also had peaks from metallic Ni crystalline phase. No other peaks were detected, indicating that i) NaCl substrate did not impaired the formation of ZnO and Ni phases; and ii) salt grains were successfully dissolved and washed off from the sample.

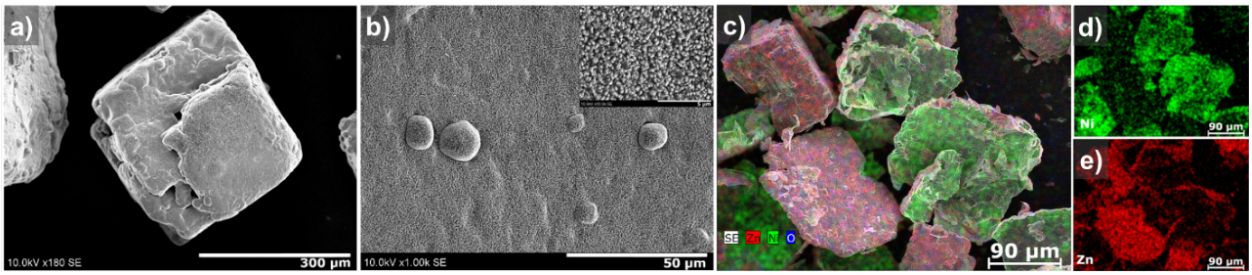

Fig. 2: SEM images of as-deposited ZnO-Ni films on NaCl grains (a and b), and EDS elemental maps of washed off bi-layered ZnO-Ni particles (c-e).

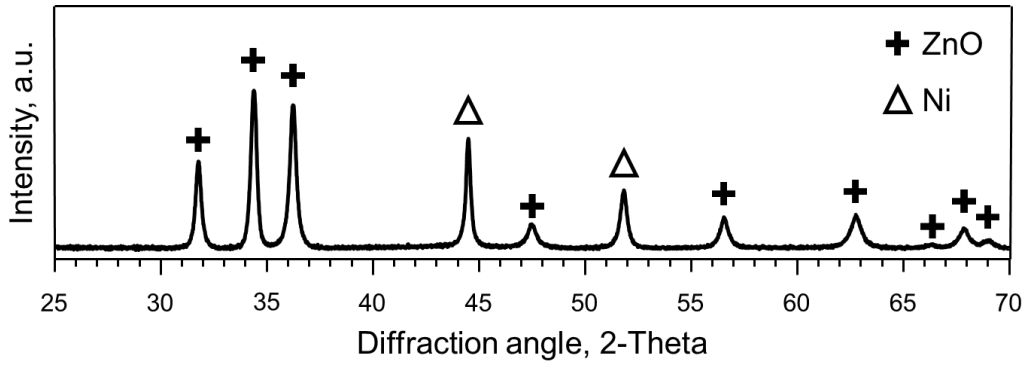

Fig. 3: XRD pattern of washed off bi-layered ZnO-Ni powder.

Fig. 4 represents the results of ten repetitive photocatalytic dye bleaching cycles using the same ZnO-Ni powder sets under UV and visible light. In general, after ten cycles ZnO-Ni powder still demonstrated relatively high activity and stability (dyes concentrations were lowered by up to 50-60 % in 3 h). But photocatalytic bleaching efficiency during the last cycle was 10-20 % lower than it was during first cycle with the fresh powder. XRD and XPS analysis (not shown here) of the used ZnO-Ni powder did not indicate any significant changes in the ZnO phase. On the other hand, XPS revealed significant build-up of the carbon species on the used powder. Furthermore, SEM analysis revealed that during cycling bi-layered ZnO-Ni particles are broken into smaller pieces which are harder to re-collect. By measuring the mass of initial and regained powder we determined that after each photocatalytic treatment cycle approximately 95 % of photocatalyst was regained. MB and RhB solutions degradation efficiency directly depends on the amount of ZnO-Ni powder. Therefore, although, the mass loss of 5 % per one cycle is not high, eventually it accumulates and results in more significant reduction of bleaching efficiency.

DOI: https://doi.org/10.26799/cp-gams2022

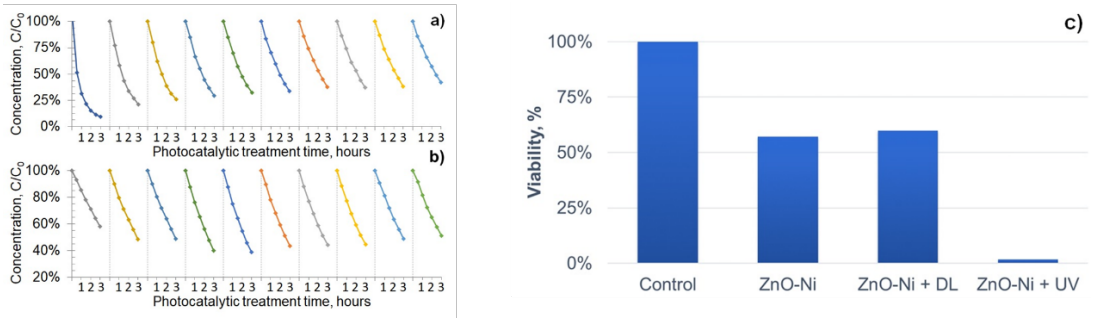

Fig. 4: Estimation of ZnO-Ni powder photocatalytic activity: a) repetitive bleaching of MB under UV, b) repetitive bleaching of RhB under visible light and c) photocatalytic inactivation of *S. Typhimurium* bacteria.

Photocatalytic inactivation of *S. Typhimurium* bacteria with ZnO-Ni powder under UV and visible light provided completely opposite results (Fig. 4c). After 1 hour treatment under UV light with ZnO-Ni bacteria viability was reduced by 98 %, but after the same time under visible light bacteria viability was not reduced at all. We assume that this might be related to the complex response of *S. Typhimurium* bacteria to the external and internal reactive oxygen species (ROS). More specifically, it is known that and if total oxidative potential of external ROS is not surpassing some certain critical level, *S. Typhimurium* bacteria are capable to adopt to the oxidative stress and well survives the photocatalytic treatment [13], [14]. Accordingly, data in Fig. 4c demonstrates that generation of ROS under UV light is enough to surpass the defensive mechanism of *S. Typhimurium*, whereas ROS generation under visible light is not.

4. Conclusion

SEM and XRD analysis confirmed that washed off bi-layered particles had crystalline ZnO on one side and metallic Ni on the other. Bi-layered ZnO-Ni particles were easily manipulated and collected by the magnetic field. On average this functionality allowed to recollect approximately 95 % of initial powder after each photocatalytic treatment test. During ten consecutive tests with UV and visible light illumination bi-layered ZnO-Ni powder maintained relatively high activity and stability. The observed 10-20 % decrease in efficiency was attributed to the partial loss of bi-layered ZnO-Ni powder and possible clamping of photocatalyst micropores. Despite this loss in efficiency, it can be concluded, that the strategy to combine ZnO particles with Ni may prove useful for the design of the reusable photocatalysts powder.

Acknowledgements

This research is funded by the European Social Fund according to the activity 'Improvement of researchers' qualification by implementing world-class R&D projects' of Measure No. 09.3.3-LMT-K-712, project "Investigation of the application of TiO_2 and ZnO for the visible light assisted photocatalytical disinfection of the biologically contaminated water" (09.3.3-LMT-K-712-01-0175). Authors are thankful for R. Uscila and M. Aikas for their valuable input in the conducted study.

References

1. D. Chen et al., "Photocatalytic degradation of organic pollutants using TiO2-based photocatalysts: A review," *J. Clean. Prod.*, vol. 268, p. 121725, 2020.
2. J. Song et al., "Visible-light-driven heterostructured g-C3N4/Bi-TiO2 floating photocatalyst with enhanced charge carrier separation for photocatalytic inactivation of Microcystis aeruginosa," *Front. Environ. Sci. Eng*, vol. 15, no. 6, pp. 129, 2021.
3. I. Dalponte Dallabona et al., "A new green floating photocatalyst with Brazilian bentonite into TiO2/ alginate beads for dye removal," *Colloids Surf. A: Physicochem. Eng. Asp.*, vol. 627, pp. 127159, 2021.

DOI: https://doi.org/10.26799/cp-gams2022

4. W. Hui et al., "In-situ synthesis of TiO2 rutile/anatase heterostructure by DC magnetron sputtering at room temperature and thickness effect of outermost rutile layer on photocatalysis," *J. Environ. Sci.*, vol. 60, pp. 33–42, 2017.
5. K. M. Lee et al., "Recent developments of zinc oxide based photocatalyst in water treatment technology: A review," *Water Research*, vol. 88, pp. 428–448, 2016.
6. A. Sreedhar et al., "Highly supportive hydrogen peroxide as a hole scavenger to improve the visible light water splitting activity of flake-like Co-doped ZnO thin films," *Solar Energy*, vol. 191, pp. 151–160, 2019.
7. N. Q. Yang et al., "Investigation of photocatalytic properties based on Fe and Ce Co-doped ZnO via hydrothermal method and first principles," *Mater. Sci. Semicond. Process*, vol. 131, p. 105835, 2021.
8. N. Daneshvar et al., "Photocatalytic degradation of azo dye acid red 14 in water on ZnO as an alternative catalyst to TiO2," *J. Photochem. Photobiol. A: Chem.*, vol. 162, no. 2, pp. 317–322, 2004.
9. M. Feygenson et al., "Properties of Highly Crystalline NiO and Ni Nanoparticles Prepared by High-temperature Oxidation and Reduction," *Phys. Rev. B,* vol. 81, pp. 014420, 2010.
10. D. Baudouin et al., "Particle size effect in the low temperature reforming of methane by carbon dioxide on silica-supported Ni nanoparticles," *J. Catal.*, vol. 297, pp. 27–34, 2013
11. M. Urbonavicius et al., "Visible-Light-Driven Photocatalytic Inactivation of Bacteria, Bacteriophages, and Their Mixtures Using ZnO-Coated HDPE Beads as Floating Photocatalyst" *Materials*, vol.15, 2022.
12. S. Varnagiris et al., "Formation of Zn-rich ZnO films with improved bulk and surface characteristics by approach of magnetron sputtering technique," *Thin Solid Films*, vol. 738, p. 138967, 2021.
13. S. Varnagiris et al., "Photocatalytic inactivation of salmonella typhimurium by floating carbon-doped TiO_2 photocatalyst," *Materials*, vol. 14, no. 19, 2021.
14. J.-J. Lee et al. "TolC is important for bacterial survival and oxidative stress response in Salmonella enterica serovar Choleraesuis in an acidic environment." *Vet. Microbiol*. vol. 193, pp. 42–48, 2016.

Proceedings of the GAMS 2022 International Conference
Paris, France – June 15 – 17, 2022
DOI: https://doi.org/10.26799/cp-gams2022

THE POSSIBILITY OF REACTIVE PRINTING ON INHERENT FLAME RETARDANT FABRICS

V. Lovreškov[1], M. I. Glogar[1], T. Kaurin1, T. Pušić[1], N. Kerman[2]

[1] Department of Textile Chemistry and Ecology, University of Zagreb Faculty of Textile Technology, Zagreb, Croatia
[2] Čateks d.d., Čakovec, Croatia

Abstract:

In this research, the analysis was performed on three selected types of inherent flame retardant fabrics whose composition and construction have been designed and developed in cooperation of Croatian textile factory Čateks d.d. and University of Zagreb Faculty of Textile Technology, in a scope of project Development of multifunctional non-flammable fabric for dual use. The warp and weft composition of the tested fabrics are as follows: warp: 95% m-AR; 5% para-AR; weft: 30% PA 6.6; 35% m-AR; 35% CV FR. The three fabric samples differ in structural characteristics: Fabric 1 is weaved in plain weave, Fabric 2 in twill 2/2, Fabric 3 in twill 3/1. The samples were subjected to a process of printing with reactive dyes, applying two concentrations of dyestuff and two types of thickeners each in two viscosities achieved with different ratios of dry matter and water. The samples were tested for flame retardancy by determining the Limited Oxygen Index (LOI), and the analysis of the print quality was performed by the test of wash fastness and colorimetric evaluation of the printed areas before and after washing. The achieved colour strength was analyzed through the objective evaluation of K/S values. The colouration of individual fabric components was analyzed by microscopic imaging of printed surfaces.

Keywords: textiles, flame retardancy, printing, reactive dyestuff, aramid, CV FR, spectrophotometry, wash fastness, microscopic imaging

1. Introduction

Due to the increasing need for inherent flame retardant fabrics in everyday life, it is necessary to find a solution that would meet the functional and aesthetic requirements of such fabrics. The complexity of the raw material composition of such fabrics complicates the process of textile printing and dyeing, and it is difficult to achieve a certain satisfactory aesthetic appearance of the fabric.

The term inherently flame retardant fabric implies achieving the property of flame retardancy without applying certain finishes that would achieve it, but the fiber structure itself achieves non-flammability. In such fabrics, meta- and para-aramid fibers, FR viscose, etc. are most often found in the yarn structure [1, 2]. Flame retardancy by itself implies the resistance to ignition and reduced flammability; the term is often synonymous with flame resistance but may be considered to relate to fabrics which ignite under a flame [3].

Since the 1950 period, the fiber industry is attempting to develop inherently flame retardant varieties, often based on aromatic structured polymeric chains. The most known examples are the aramids and the poly(meta-aramid) fiber appeared commercially in the 1960 period under trade name Nomex® produced by Du Pont, followed by the poly (para-aramid) fibre Kevlar® (Du Pont) in the late 1960s as a high tenacity and modulus fiber which possessed superior heat and fire resistance [4].

Zhao et al. investigated the flame retardant property of Nomex/Lenzing Viscose FR fabric with different blend ratios. They stated that, the blended fabric of two fibers have better flame retardant property than that of pure fabric of each fiber [5].

Sonee et al., also researched the flame retardancy of fabric structured of meta aramid, FR viscose and PA 6,6 in blends of different ratios. Their results showed that the best flame retardant behavior have the blend of FR viscose/meta-aramid 70:30, while the blends with PA 6,6 are having lower LOI indicating the lower flame retardant properties [6].

DOI: https://doi.org/10.26799/cp-gams2022

In this paper, the possibility of using reactive dyes in the printing of inherently non-combustible fabrics that contain a high proportion of aramid fibers was examined. Reactive dyes are the most important class of dyes since they can be linked onto the textile fibers through covalent bonds, obtaining the high fastness to wet treatment [7]. In reactive dyes, azo dyes and anthraquinone dyes are the most important groups. The azo dyes are characterized by a simple mode of synthesis and high molar absorption coefficient, although they are not showing, in general, the satisfactory light stability. The anthraquinone dyes, on the contrary are having excellent light fastness properties [7, 8].

With washing and light fastness testing, samples were also tested for flame resistance by Limiting Oxygen Index (LOI) which is a minimum percent of oxygen in the environment that sustains burning under specified test conditions. In other terms, it is the content of oxygen in an oxygen-nitrogen mixture that keeps the sample at the limit of burning [9]. Protective clothing should be breathable and smooth, easy to wear and maintain body temperature, therefore the expected result is inherent flame retardant fabric that, due to the avoidance of layering and finishing, will have better comfort properties and better resistance to washing.

The samples were printed using the screen printing technique with pastes of different concentrations of dyes in order to achieve different depth of color, and thus we are testing the possibility of printing the problematic fire-resistant yarn contained in the composition of the fabrics.

2. Experimental

The research was conducted on three non-commercial fabrics whose structural properties and composition were designed and developed in cooperation with the Croatian Textile Factory Cateks and the Faculty of Textile Technology of the University of Zagreb. Fabric 1 was in plain weave, Fabric 2 was in twill 2/2 and Fabric 3 was in twill 3/1 weave. All three fabrics have the same composition, shown in Table 1, the warp threads are a mixture of meta-aramid, m-AR (95%) and para-aramid, p-AR (5%), while the weft threads differ in composition, polyamide 6.6 (PA), FR viscose (CV FR) and meta-aramid (m-AR).

Table 1. Composition of fabrics.

	Fabric 1	**Fabric 2**	**Fabric 3**
Weave	Plain	Twill 2/2	Twill 3/1
Warp	95% M-Armaid; 5% P-Aramid		
Weft	30% PA 6.6; 35% Lenzing FR; 35% M-Aramid		

Structural and mechanical properties of the fabrics are shown in Table 2.

Table 2. Constructional and mechanical characteristics of fabrics.

	Mass [g/m²]	**Thickness 0.5 kPa [mm]**	**Thickness 1 kPa [mm]**	**Warp Density [threads/cm]**	**Weft Density [threads/cm]**
Fabric 1	210,38	0,70	0,66	39	19
Fabric 2	205,70	0,79	0,76	38	20
Fabric 3	201,63	0,86	0,83	38	20

DOI: https://doi.org/10.26799/cp-gams2022

The samples were woven on a FANYUAN INSTRUMENT DW598 pattern weaving machine, a fully automated woven bar pattern weaving loom. The loom is characterized by a maximum base width of 50 cm; number of wefts per minute from 30 to 60 and with a maximum number of sheets of 20.

2.1. LOI (Limiting Oxygen Index)

The fabrics were tested for flame retardance by LOI—Limiting Oxygen Index, measured using Limiting Oxygen Index Apparatus (Concept Equipment Ltd., Angmering, UK) according to EN ISO 4589-2: 2017 Plastics-Determination of burning behavior by oxygen index-Part 2: Ambient-temperature test. Samples in size 140 mm × 53 mm were conditioned (RH 65%, 24 h) according to standard ISO 139:2008/A1 Textiles-Standard Atmospheres for Conditioning and Testing, the calculation shown in equation (1).

$$LOI = \frac{O_2}{H_2+O_2} \times 100 \quad (1)$$

2.2. Screen printing of inherent flame retardant fabrics

The fabrics were printed with reactive dyes using the screen printing technique. For the preparation of printing pastes, a reactive dye and two thickeners were used, each in two different viscosities defined by the ratio of water to dry matter. The first thickener was CHT-Alginat MV (CHT Group and Co) and the second Alkagum NS (Diamalt AG, München, Germany). Both were prepared in 4% and 9% of a thickening agent (dry matter), so different viscosities were tested. The reactive dyestuff used was Brilliantblau V-R spez, Bezema (C.I. Reactive Blue 19, C.I. 61200), in two concentrations. Pastes with a lower concentration of dye are marked with a letter "a", and pastes with a higher concentration of dye with "b". The composition of the printing pastes is shown in Table 3. Quantities of components in printing pastes are shown per 100g of printing paste. The samples were printed by hand screen procedure, fixed and dried with steam for 10 min.

Table 3. Composition of printing pastes

Paste	**Thickener**		**Dyestuff**	**Urea**	**Na_2CO_3**
1a	CHT-ALGINAT MV (4%)	50 g	1,26 g	20 g	4g
2a	CHT-ALGINAT MV (9%)	50 g	1,26 g	20 g	4g
3a	Alkagum NS (4%)	50 g	1,26 g	20 g	4g
4a	Alkagum NS (9%)	50 g	1,26 g	20 g	4g
1b	CHT-ALGINAT MV (4%)	50 g	7,5 g	20 g	4g
2b	CHT-ALGINAT MV (9%)	50 g	7,5 g	20 g	4g
3b	Alkagum NS (4%)	50 g	7,5 g	20 g	4g
4b	Alkagum NS (9%)	50 g	7,5 g	20 g	4g

2.3. Colorimetric Analyses

Colour characteristics were measured using a remission spectrophotometer, Datacolor 850, measuring geometry d/8°, D65, measuring aperture of 9 mm. All results were measured on samples by repeating the measurement procedure at random locations on the samples. Thus, the colour measurements were made using the Datacolor Tools computer program and "Measuring until tolerance" command, which means that at least 10 measurements must be made, and the results are accepted only if the total colour difference between each measurement is less than 0.1 (dE* < 0.1).

2.4. Wash Fastness Testing and Spectrophotometric Measurement

DOI: https://doi.org/10.26799/cp-gams2022

Wash fastness testing was performed in a laboratory apparatus Polycolor, Mathis according to standard ISO 105-C06:2010 (A2S) Textiles—Tests for color fastness—Part C06: Colour fastness to domestic and commercial laundering, using 5 g/L standard detergent (ECE Non phosphate detergent without optical brightener agent), with bath ratio 1:8, temperature 40 ± 2 °C, time 30 min, through 5 cycles. The samples were air dried between each cycle.The wash fastness of the print was assessed by spectral evaluation of the sample before and after washing using DataColor 850 spectrophotometer with constant instrument aperture, standard light D65 and d/8 ° geometry. The results are shown as a color difference value calculated according to the CIE76 formula.

2.5. Microscopic Imaging

Microscopy of the printed sample was performed using DinoLite AM7013 at 50x magnification. Imaging was performed before and after the fifth wash. Microscopic imaging was performed using the following parameters: Magnification: 50×/1.3MP. Unit: mm; Horizontal FOV [Accuracy]: 9.564 mm [+/- 0.192 mm]; 1 pixel step (1 keystroke on keyboard): ~ 7.4 µm). The scanning of the fabrics was performed with resolution of 1200 dpi.

3. Results and discussion

Flame retardant properties of fabrics before printing, determined by measuring LOI-Limiting Oxygen Index are presented in Table 4. The criteria specified for the inherently flame-retardant fabrics is LOI > 26% (percent of oxygen), so the results show satisfactory property.

Table 4. LOI of fabrics; minimal percent of oxygen.

		Fabric 1	Fabric 2	Fabric 3
LOI [%]	**Warp**	31,40	31,60	31,70
	Weft	31,48	31,51	31,51

Figures 1-3 show microscopic images of printed fabrics. It was observed that the binding of dyes in the process of printing and fixing occurs only on the viscose component of the yarn, while the aramid component remained undyed.

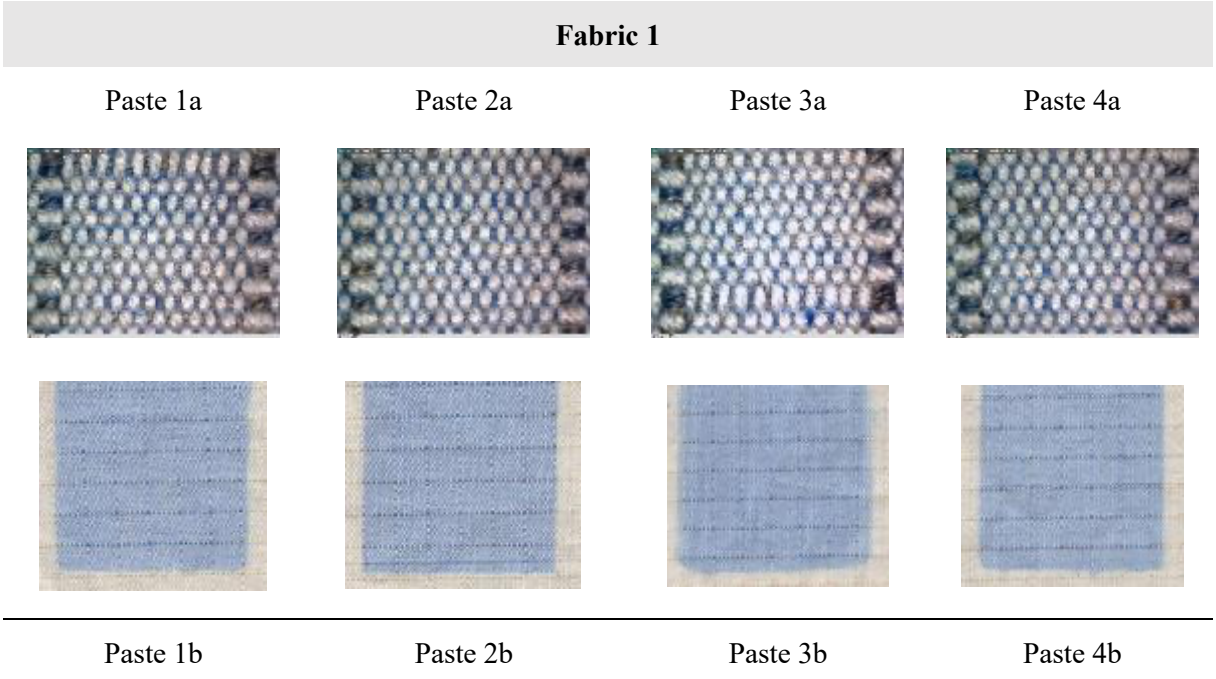

DOI: https://doi.org/10.26799/cp-gams2022

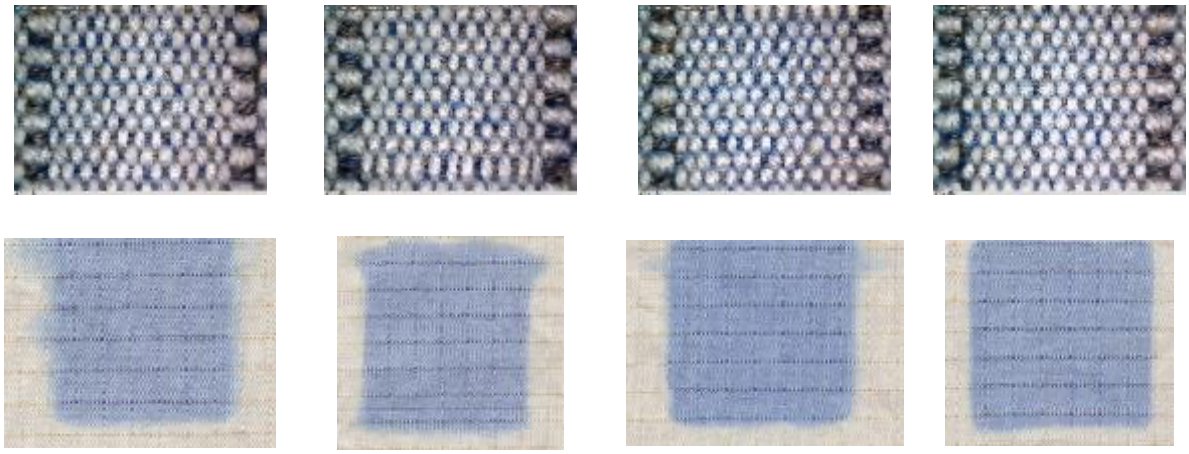

Figure 1. DinoLite microscopic and scanned images of printed Fabric 1.

The images of the printed samples show the appearance of the achieved colouration. The quality of the print is defined by the sharpness of the print and the achieved color characteristics. Satisfactory print sharpness was achieved for samples printed with paste 2a, 4a and 4b. Regardless of the type of thickener, the result shows that for this type of fabric a thickener with a higher proportion of dry matter is suitable. Microscopic images show that part of the aramid yarn remained undyed, and it is visible due to the weaving characteristics. The simultaneous interaction of the remission of the colored and undyed components of the fabric can affect the final appearance of the color of the fabric.

Fabric 2

Paste 1a | Paste 2a | Paste 3a | Paste 4a

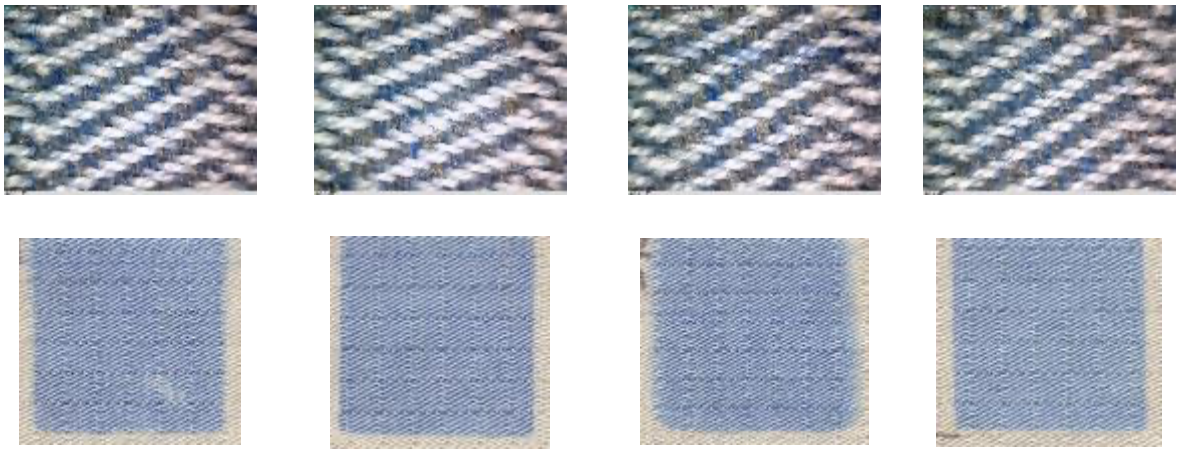

Paste 1b | Paste 2b | Paste 3b | Paste 4b

DOI: https://doi.org/10.26799/cp-gams2022

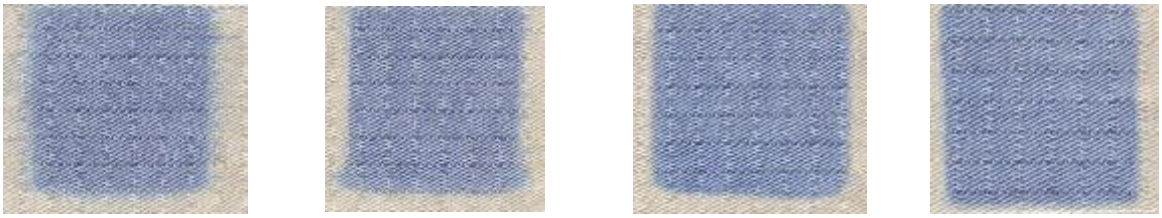

Figure 2. DinoLite microscopic and scanned images of printed Fabric 2.

Fabric 2 and Fabric 1 differ in the type of weave, which also affects the behavior of the printing paste. With Paste a, regardless of the type of thickener and the amount of dry matter, a satisfactory sharpness of the print was obtained, but for Paste b, where a larger amount of dye is present (recipe in table 3), for the CHT-Alginate MV thickener, the printing paste spread beyond the pattern contour. A starch-based thickener (Alkagum NS) proved to be more suitable for printing on Fabric 2 with a higher color concentration.

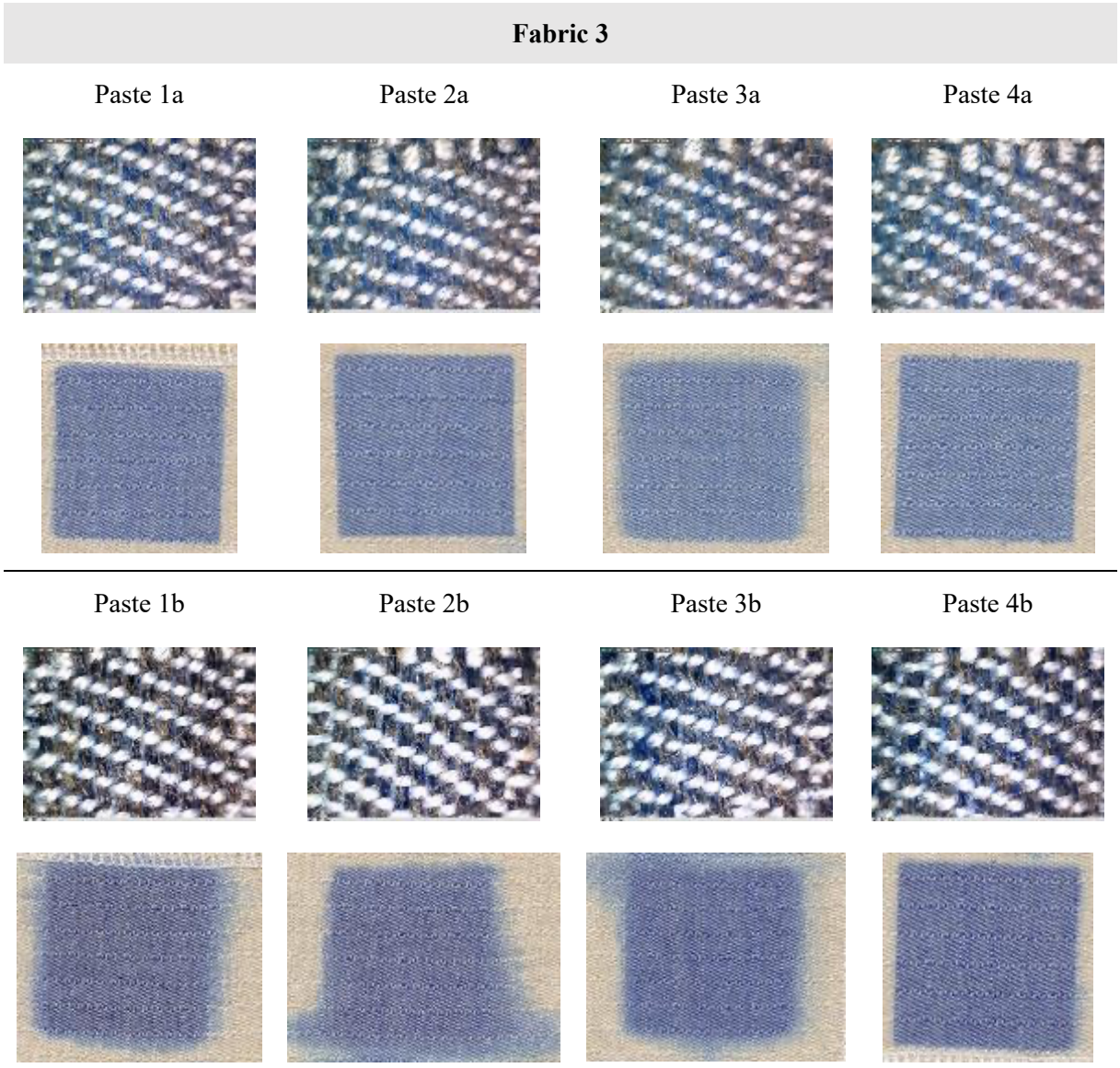

Figure 3. DinoLite microscopic and scanned images of printed Fabric 3.

A similar trend of differences is observed for Fabric 1 and 2. For Paste b, which is characterized by a higher proportion of dyestuff, spreading of dye outside the print contour is observed. On microscopic

DOI: https://doi.org/10.26799/cp-gams2022

images it is observed for samples printed with the same Paste b, a darker color of the dye-binding component, which is associated with the occurrence of dye capillary spreading. Saturation occurred in viscose component that has an affinity for the reactive dye, which resulted with maximum dye binding, and with the excess dye capillary spillage. With the lower dye content, satisfactory print sharpness was obtained for recipes with a higher viscosity thickener meaning a higher dry matter content (Paste 2a and 4a), regardless of the type of thickener. As for Pastes b with a higher dye content, a satisfactory print sharpness is obtained for printing pastes 4 with a starch-based thickener (alkagum NS).

Microscopic images of fabrics 1, 2 and 3 clearly show the difference in the weave structure resulting in the difference in the ratio of colored and undyed components in the composition of the fabric, such a ratio affects the subjective appearance of the color as well as the objective measurements that follow.

Comparative analysis is given of the objective values of color strength (K/S) and the ratio of lightness (L*) and chroma (C*) as a definition of color intensity. The results of K/S are shown graphically in Figure 4, and the L*/C* values are shown in Table 5.

Table 5: Lightness (L*) and chroma (C*) relationship for printed samples, as definition of colour intensity.

	L*	**C***		**L***	**C***
Fabric 1 Paste 1a	64,96	8,17	Fabric 1 Paste 1b	63,85	9,33
Fabric 1 Paste 2a	63,31	7,23	Fabric 1 Paste 2b	61,69	10,02
Fabric 1 Paste 3a	65,05	7,87	Fabric 1 Paste 3b	65,15	8,35
Fabric 1 Paste 4a	63,34	7,17	Fabric 1 Paste 4b	62,69	8,42
	L*	**C***		**L***	**C***
Fabric 2 Paste 1a	61,49	8,83	Fabric 2 Paste 1b	60,99	9,06
Fabric 2 Paste 2a	59,35	7,42	Fabric 2 Paste 2b	60,06	8,56
Fabric 2 Paste 3a	61,48	8,27	Fabric 2 Paste 3b	62,89	8,23
Fabric 2 Paste 4a	60,34	6,89	Fabric 2 Paste 4b	60,70	7,96
	L*	**C***		**L***	**C***
Fabric 3 Paste 1a	53,43	9,88	Fabric 3 Paste 1b	54,99	9,99
Fabric 3 Paste 2a	50,21	6,88	Fabric 3 Paste 2b	49,80	10,35
Fabric 3 Paste 3a	54,01	10,28	Fabric 3 Paste 3b	55,16	10,13
Fabric 3 Paste 4a	51,00	7,60	Fabric 3 Paste 4b	50,94	9,85

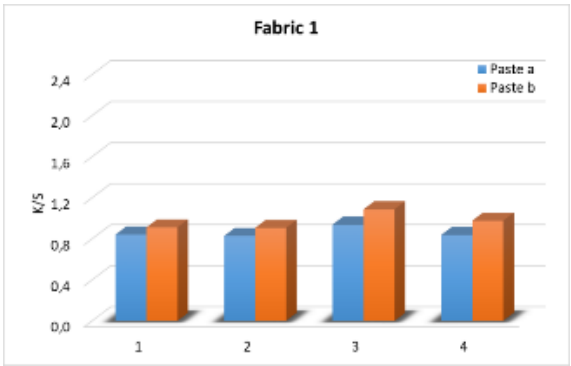

(a)

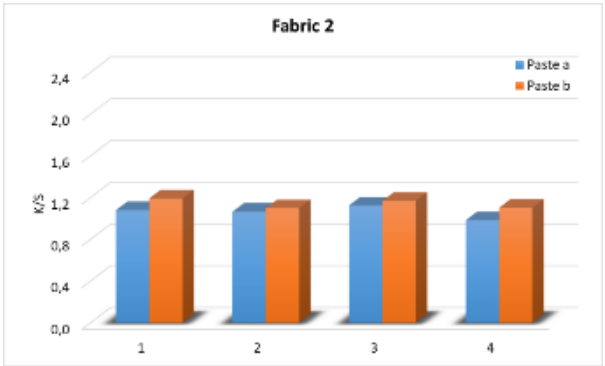

(b)

Proceedings of the GAMS 2022 International Conference
Paris, France – June 15 – 17, 2022
DOI: https://doi.org/10.26799/cp-gams2022

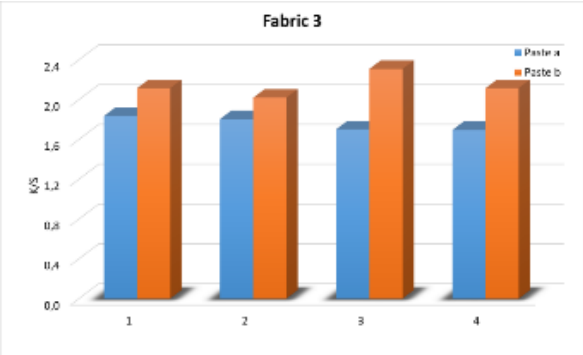

(c)

Figure 4. K/S objective values of color of printed surfaces: Fabric 1 (a), Fabric 2 (b) and Fabric 3 (c).

Objective K/S values show a relatively low achieved color strength. Slightly higher values were obtained for printing pastes "b" with a higher concentration of dyestuff. Such lower K/S values were to be expected, given that only a partial ratio of components contained in the yarn composition is capable of bonding with dyestuff (the cellulosic part contained in the viscose yarn component). The properties and quality of the print are analyzed using spectrophotometry. In dye printing, achieving a satisfactory intensity and brilliance of coloration of printed parts of the fabric is very complex. In the samples tested in this study, the lower intensity of the obtained coloration is contributed by the specific composition of the fabric in which more than half of the content are fibers that cannot be dyed by the process of dye-fiber chemical bonding.

The values of color depth (K/S), lightness (L*) and chroma (C*) of the samples before and after the fifth wash were compared. The results for K/S after 5 washing cycles are shown graphically on Figure 8 and the results for lightness (L*) and chroma (C*) are given in Table 6.

Figure (5-7). Microscopic and scanned images of Fabric 1, Fabric 2 and Fabric 3 (printed with Paste a and Paste b), after 5 washing cycles.

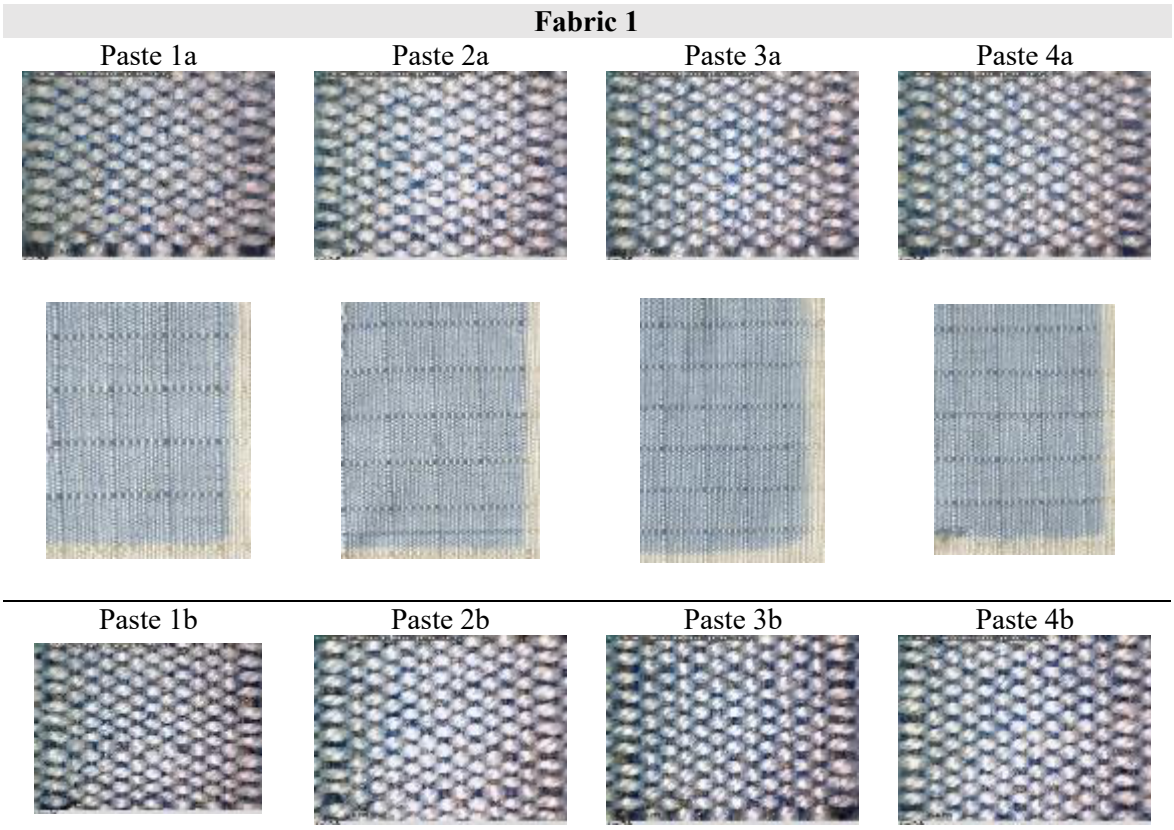

DOI: https://doi.org/10.26799/cp-gams2022

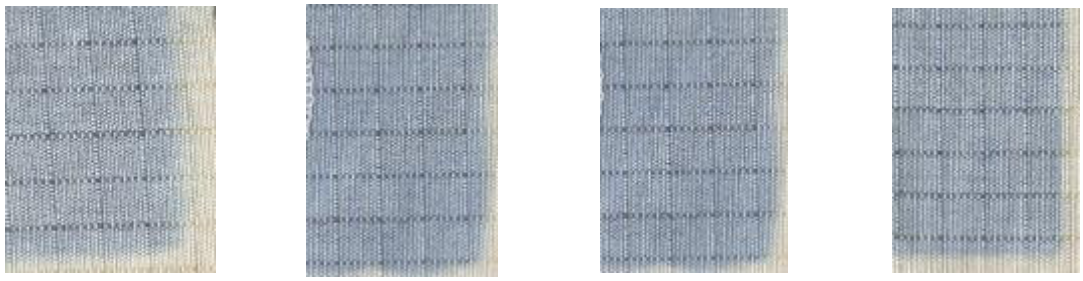

Figure 5. DinoLite microscopic and scanned images of printed Fabric 1 after 5 washing cycles.

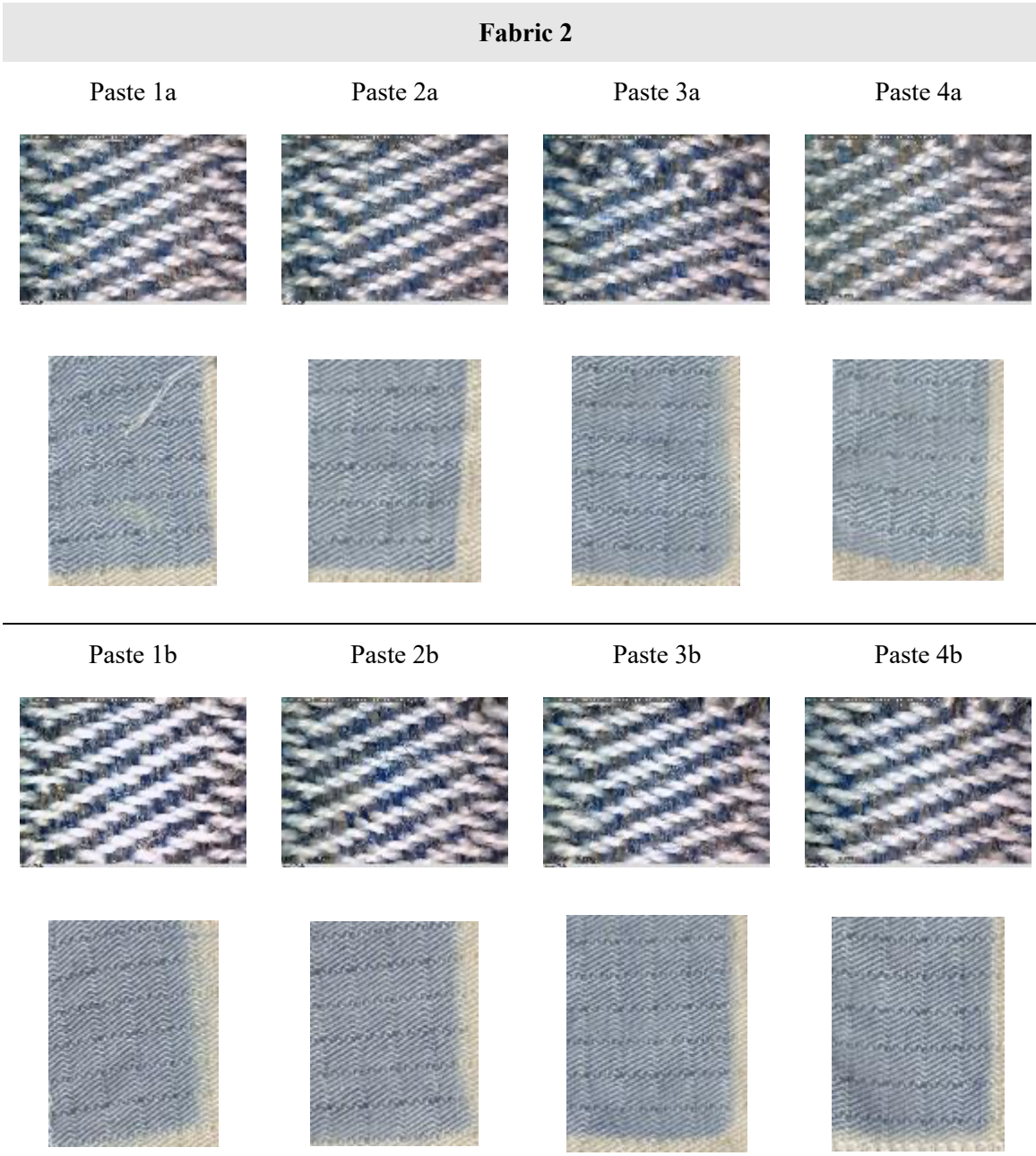

Figure 6. DinoLite microscopic and scanned images of printed Fabric 2 after 5 washing cycles.

DOI: https://doi.org/10.26799/cp-gams2022

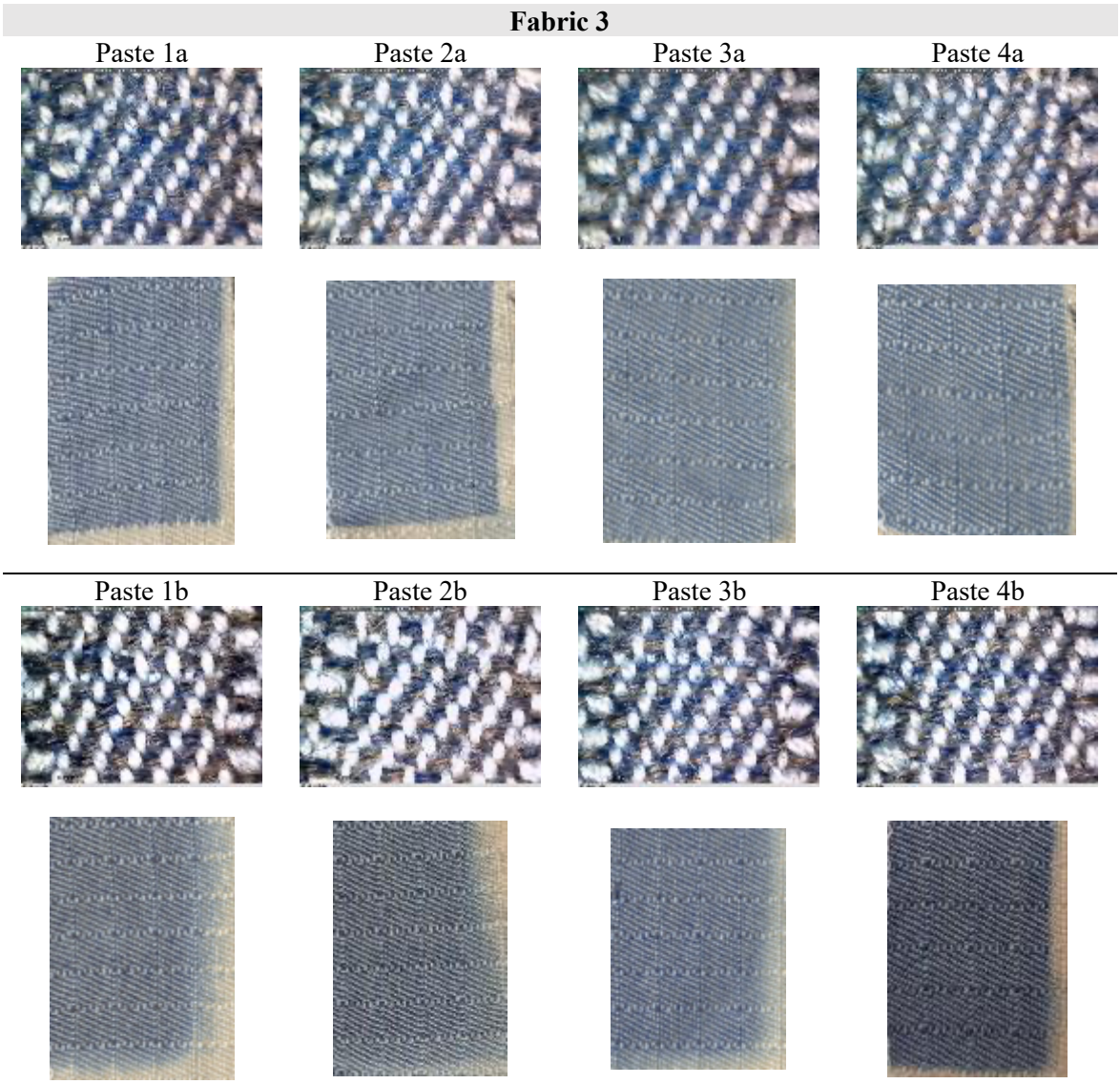

Figure 7. DinoLite microscopic and scanned images of printed Fabric 3 after 5 washing cycles.

The results after 5 washing cycles carried out in the process of testing the durability of the print on washing show certain changes. Noticeable differences were obtained in the strength of the K/S color whose value decreased after 5 washing cycles.

Table 6: Lightness (L*) and chroma (C*) of printed samples after 5 washing cycles.

	L*	**C***		**L***	**C***
Fabric 1 Paste 1a	68,23	6,70	Fabric 1 Paste 1b	64,36	6,06
Fabric 1 Paste 2a	67,34	6,47	Fabric 1 Paste 2b	63,70	6,22
Fabric 1 Paste 3a	65,04	8,27	Fabric 1 Paste 3b	61,50	8,76
Fabric 1 Paste 4a	66,38	7,25	Fabric 1 Paste 4b	63,29	7,38
	L*	**C***		**L***	**C***
Fabric 2 Paste 1a	62,47	7,73	Fabric 2 Paste 1b	59,85	6,36
Fabric 2 Paste 2a	61,97	7,31	Fabric 2 Paste 2b	61,30	5,86
Fabric 2 Paste 3a	61,38	8,03	Fabric 2 Paste 3b	60,50	7,44
Fabric 2 Paste 4a	64,12	7,20	Fabric 2 Paste 4b	61,27	7,05
	L*	**C***		**L***	**C***
Fabric 3 Paste 1a	54,01	9,28	Fabric 3 Paste 1b	51,08	6,42

DOI: https://doi.org/10.26799/cp-gams2022

Fabric 3 Paste 2a	54,33	9,57	Fabric 3 Paste 2b	52,21	6,95
Fabric 3 Paste 3a	55,84	8,95	Fabric 3 Paste 3b	50,62	9,84
Fabric 3 Paste 4a	56,23	8,95	Fabric 3 Paste 4b	51,34	9,08

A lower value of chroma (C*) confirms the influence of undyed aramid fibers in the yarn, which certainly reduces chromaticity (C*), and increases lightness (L*) due to the pronounced reflection from undyed parts of the yarn.

Color differences are calculated on the basis of objective spectrophotometric measurement of print samples before and after 5 washing cycles, with the standard (reference) values being those of printed unwashed samples. The results are presented as differences in color parameters (lightness difference dL*, color difference dC* and hue difference dh) as well as in terms of the total color difference value (dE), graphically on Figure 9.

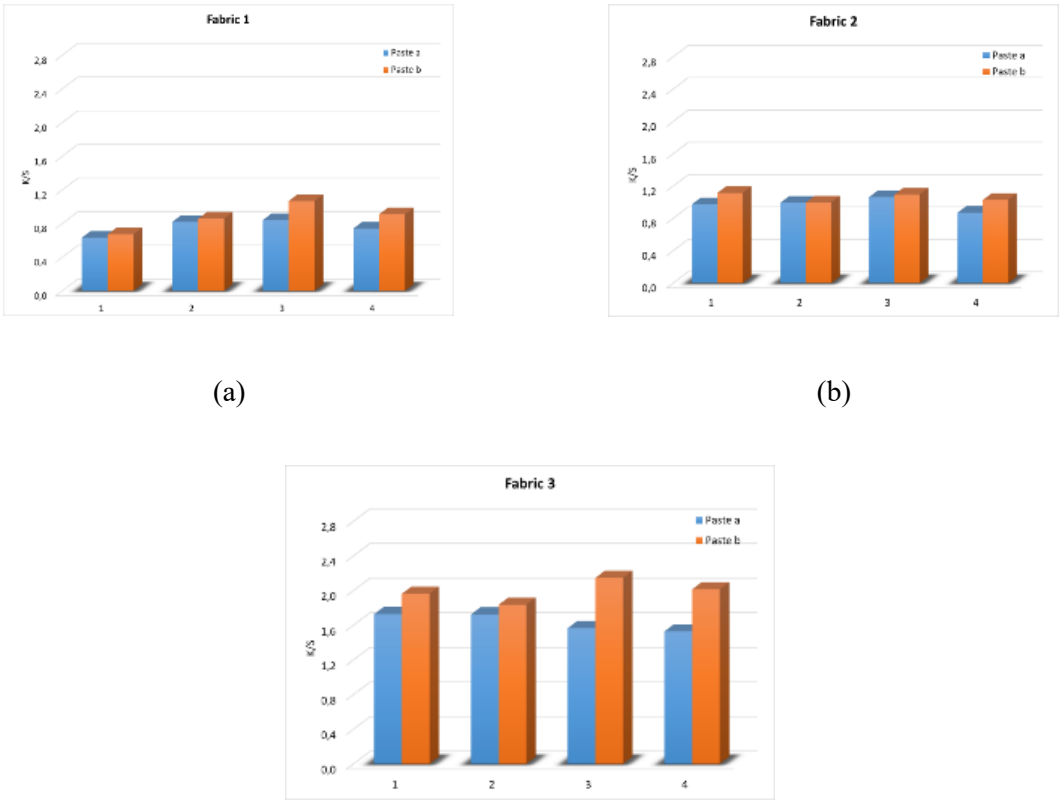

(a) (b)

(c)

Figure 8. K/S objective values of color of printed surfaces after 5 washing cycles: Fabric 1 (a), Fabric 2 (b) and Fabric 3 (c).

In the washed samples of Fabric 1, Fabric 2 and Fabric 3, a slight change in color depth (K/S) was obtained after 5 wash cycles, indicating that there was no visible color release.

For the ratio of lightness (L*) and chroma (C*), in general for all samples (fabrics 1 to 3), an increase in lightness (L*) and a decrease in chroma (C*) were observed. An increase in lightness and decrease in chroma indicates a shift in color towards a lighter, which indicates on a slight but still faded color caused by the washing process.

Proceedings of the GAMS 2022 International Conference
Paris, France – June 15 – 17, 2022
DOI: https://doi.org/10.26799/cp-gams2022

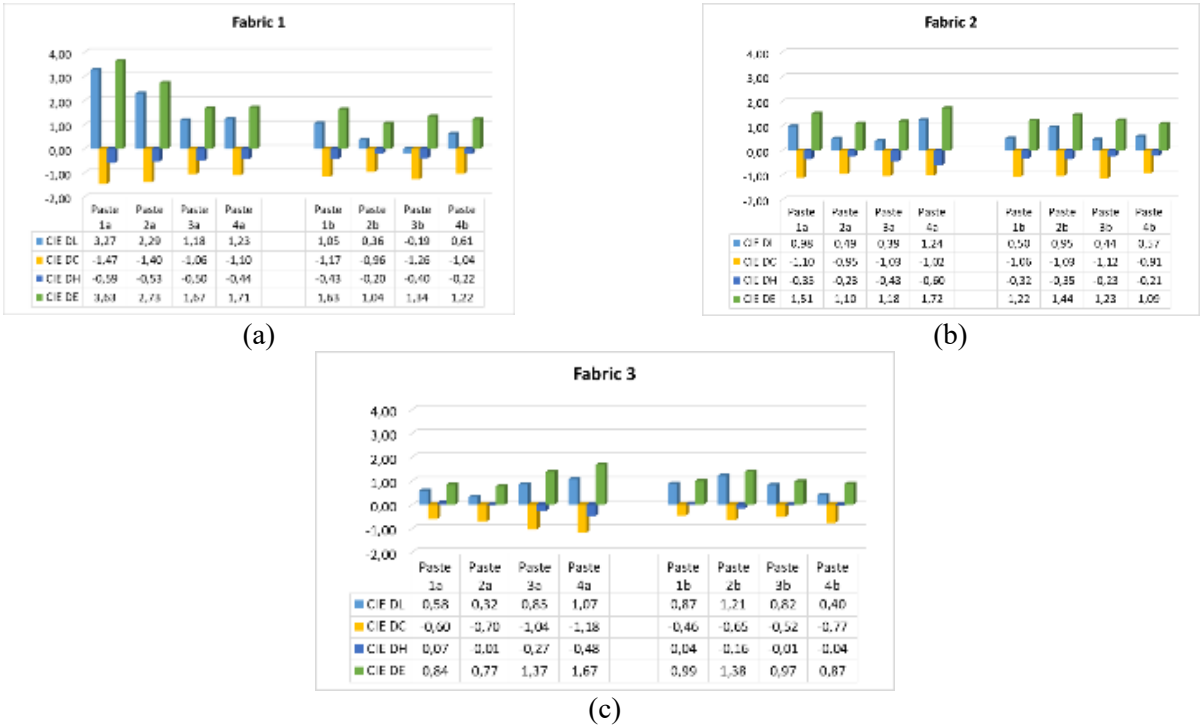

Figure 9. Color differences values calculated according to CIE76 formula of Fabric 1 (a), Fabric 2 (b) and Fabric 3 (c). Comparing values of unwashed samples with values obtained after 5th wash cycle.

In order to confirm the washing stability of reactive dyes prints, an analysis of color differences calculated according to the CIE76 formula was carried out, taking the unwashed sample as a reference and comparing it with the samples after the 5th washing cycle (Table 5). The results are presented as differences in individual color parameters (dL* - difference in brightness, dC* - difference in color; dh - difference in color shade) and as the value of the total difference in color, dE. A visibly larger difference was obtained in the brightness parameter of the Fabric 1 sample with Paste 1a and Paste 2a, significantly outside the permitted tolerance limit (dL*<1.5). The differences obtained in the chroma C* and hue h° parameters are insignificant. Almost all values of differences in lightness (dL*) are within the tolerance limits, values of total color differences (dE) are within the allowed ranges (dE≤1.5-2) except for the Paste 1a and Paste 2a print samples of Fabric 1. The results of the differences are acceptable and indicate a satisfactory color wash fastness.

After 5 washing cycles, a test of color fastness to light was also carried out. The results are expressed in blue scale grades, and are shown graphically in Figure 10. The results show low fastness to light, with no difference related to the concentration of dyes in the printing paste

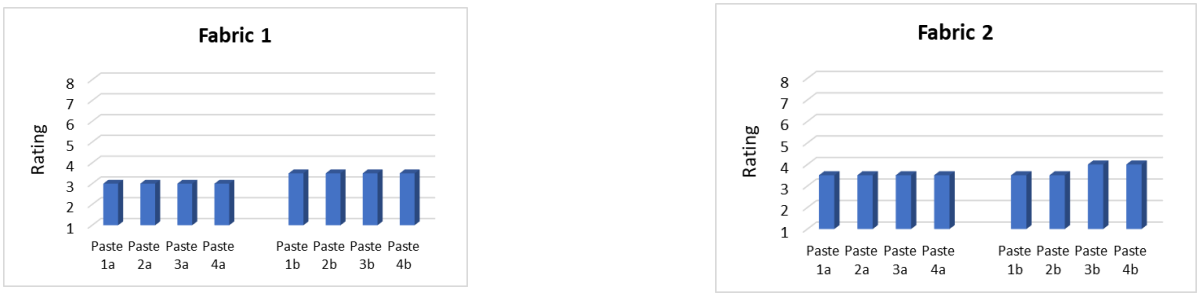

DOI: https://doi.org/10.26799/cp-gams2022

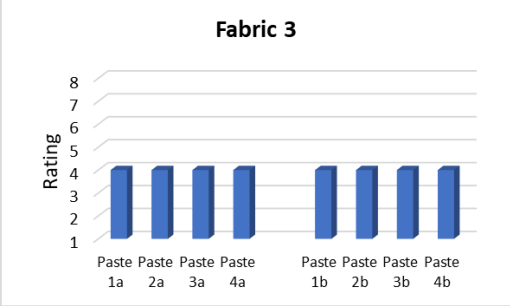

(c)

Figure 10: Blue scale grades for samples of Fabric 1 (a), Fabric 2 (b) and Fabric 3 (c) printed with Paste a, and Paste b, washed after 5th cycle

4. Conclusions

Based on the results of the analysis, it can be confirmed that there is a possibility of achieving a certain level of coloration in inherently fire-resistant fabrics that contain a high proportion of aramid fibers (95% in the composition of the warp and 35% in the composition of the weft), with a certain ratio of viscose (35% in the weft yarn), which has the ability of binding the reactive dye. Although the objective evaluation of the color intensity yielded lower K/S values (1.1 to 2.3), the analysis of the relationship between the parameters of color lightness (L*) and chroma (C*), achieved satisfactory coloring (maximum values of L* = 65, 15 and C* = 10.35). The results confirmed the optimal washing fastness in the process of five washing cycles, more emphasized for Fabric 3, where for all printing conditions (type and viscosity of thickener as well as colorant content) the smallest difference values were obtained (dECIE = 0.84–1.67). Satisfactory bonding of the dye was achieved, and the washing fastness test confirmed that during 5 washing cycles, no significant fading of the color occurs. Lower lightfastness was obtained, which is expected for fabrics with a higher proportion of aramid fibers in the yarn, which generally have poor lightfastness, but also for reactive dyes.

Acknowledgment: This work has been supported by the European Union from the European Regional Development Fund under the project KK.01.2.1.02.0064 Development of multifunctional non-flammable fabric for dual use.

References

1. Horrocks, A. R.: Inherently Flame-resistant Fibres, In *Update on Flame Retardant Textiles: State of the Art, Environmental Issues and Innovative Solutions*, Smithers Rapra Technology Ltd, ISBN 978-1-90903-017-6, UK, (2013), 179-203.
2. Alongi, J.; Carosio, F.; Horrocks Richards, A.; Malucelli, G. Update on Flame Retardant Textiles: State of the Art Environmental Issues and Innovative Solutions; A Smithers Group Company: UK, 2013; pp. 1–14.
3. Bourbigot, S. Flame retardancy of textiles: new approaches. In Advances in Fire Retardant Materials; Horrocks, A.R.; Price, D.; Eds.; Woodhead Publishing: Cambridge, UK, 2008; pp. 9–40.
4. Horrocks, R. A.: Flame Retardant Challenges for Textile and Fibers: New Chemistry Versus Innovatory Solutions, *Polymer Degradation and Stability*, 96 (2011), 377-392, ISSN 0141-3910
5. Zhao, S.; Hong-li, D.: Influence of Blending ratio of Nomex/Lenzing Viscose FR on Flame-retardant Property of the Fabric, *Journal of Textile Research*, 27 (2006) 12, 74-76, ISSN 0253-9721
6. Sonee, N.; Arora, C.; Parmar, M. S.: Burning Behaviour of Aramid and FR Viscose Blended Fabrics, *Indian Journal of Fibre & Textile Research*, 44 (2009), 238-243, ISSN 09710426
7. Shan, B. et al.: A New Kind of H-Acid Monoazo-Anthraquinone Dyes with Surprising Colour, *Dyes and Pigments*, 123 (2015), 44-54, ISSN 0143-7208
8. Epolito, W. J. et al.: Characterization of the Textile Anthraquinone dye Reactive Blue 4, *Dyes and Pigments*, 67 (2005), 35-46, ISSN 0143-7208
9. Chowdhury, A. K. R. *Flame Retardants for Textile Materials*; CRC Press, Boca Raton, 2020, 19.

Proceedings of the GAMS 2022 International Conference
Paris, France – June 15 – 17, 2022
DOI: https://doi.org/10.26799/cp-gams2022

Surface properties of polyester fabrics

Ana Šaravanja[1], Tihana Dekanić[1], Tanja Pušić[1], Tea Kaurin[1], Katia Grgić[1], Mirjana Čurlin[2]

[1] Department of Textile Chemistry and Ecology, University of Zagreb Faculty of Textile Technology, Zagreb, Croatia, ana.saravanja@ttf.unizg.hr
[2] Department of Process Engineering, University of Zagreb Faculty of Food Technology and Biotechnology, Zagreb, Croatia

Abstract

Large amounts of plastics used for a different purposes caused a certain environmental problems. Analysis of microplastic samples (MP) from the environment, shown that textile fibres are common source of pollution.This study was focused on the characterization of standard polyester fabric after exposure to artificial aging and 10 washing cycles. The study addressed two issues: impact of artificial light and wash media on the surface properties of polyester fabrics and applicability of multivariate analysis (MVA) for assessment of polyester samples before and after exposure to light and washing.

Keywords: microplastic, washing, textiles, polyester, polyester ageing

1. Introduction

Large amounts of water are used in the textile industry for pre-treatment and treatment of textile materials. As a consequence of all these processes, a huge amount of waste water is generated. Waste water is heterogeneous in its composition and must be purified before it can be reused. If the composition of waste water is observed, various substances from all production processes can be found in it. The most common substance found in wastewater is microplastic (MP). Due to its slow biotic decomposition, plastic is distributed in the environment, which is an undesirable effect. This type of plastic can be found in the environment for weeks, months, or years, where it is fragmented by photochemical and mechanical processes, resulting in MP (<5 mm) and nanoplastics (<1 μm) [1].

Generally speaking, it is well-known that five parameters participate in the washing process: water, soil, textile material, detergent, and washing machine. Water is the medium where the washing process is carried out and also enables the transport of heat and mechanics during process. Sinner's cycle concept describes the washing process, which is a result of a combination of four factors: mechanics, physical-chemical action, time, and temperature, Fig. 1 [2].

Fig. 1. Washing factors according to Sinner's cycle: time, temperature, mechanics and chemistry.

Polyester fibres, PES, belong to the group of fibres formed from macromolecules of synthetic polymers with a linear structure and characterised by ester bonds (- CO -O-). Poly(ethylene terephthalate), PET, is the most popular polymer in the group of polyester fibres. In 2017, PET accounted for 50% of the total production of synthetic fibres, and only 14% of it was recycled PET [3]. In general, PET has a density of 1.37-1.45 g cm-3, sinks quickly, is not biodegradable and has been found to be resistant to

DOI: https://doi.org/10.26799/cp-gams2022

atmospheric conditions. PES is not hazardous to human health and the environment, but its properties (high volume fraction in waste and high resistance to atmospheric and biological conditions) place it in the category of environmentally unacceptable materials.

When mentioning the concept of microplastic release during the washing process, it should be noted that this problem is directly related to textiles made of synthetic fibres. The most common representative of synthetic fibres is the PES fibre. Previous studies have investigated the release of microfibres during and after washing of polyester textiles at different parameters such as time, mechanical action, temperature and amount of detergent. The results showed that the average fibre diameter varied between 11.9 and 17.7 μm and the length between 5.0 and 7.8 mm [4]. The annual release of polyester microfibres in Finland is estimated at 154000 kg [5].

In the concept of the ageing process of textile material, two types of ageing are considered: chemical and physical ageing. Chemical ageing occurs as a response to a reaction with external substrates such as oxygen, solar UV radiation or water [6]. Physical ageing is caused by changes in composition, water absorption and, in addition to composition, changes can also occur in the chain configuration. As an example of physical ageing, the solvent penetration reaction or the reduction of plasticisers are mentioned [6]. Water has the ability to react with ester groups, leading to physical ageing. It is a reversible process that causes damage that occurs in the interior or on the surface of the fibres [6-9].

The aim of this research was to study the influence of artificial ageing on standard polyester fabric washed through 10 washing cycles. The study addressed two issues: the impact of artificial light and washing media on the surface properties of polyester fabrics; and the applicability of multivariate analysis (MVA) for assessment of polyester samples before and after exposure to light and washing.

2. Experimental

The standard polyester fabric (U), supplied by the Center for Test Materials, CFT, Netherlands was used. The fabric characteristics are shown in Tab. 1.

Tab. 1. Characteristics of the standard polyester fabric

Supplier (CFT)	PN-01
Color	white
Surface mass (g/m^2)	156.0
Density (thread /cm) warp weft	 27.7 20.0
Thickness (mm)	0.35
Fineness (tex) warp weft	 30.4 31.9
Weave	plain

The fabrics were subjected to 10 washing cycles (W) in Rotawash, SDL Atlas, according to HRN EN ISO 6330:2012 with reference standard detergent without phosphate with liquid ratio (LR) 1:8 temperature 60°C and,time 30 min. Artificial aging (A) was up to 75 hours according to ISO 105-B02:2013, Fig. 2.

DOI: https://doi.org/10.26799/cp-gams2022

a.)

b.)

Fig. 2: Apparatus for process: a.) Rotawash, b.) Xenotest 440

Surface characterisation of untreated, washed and aged polyester fabrics was done by scanning electron microscope FE-SEM Mira LMU, Tescan, Czech Republic. The samples were analysed using a SEM operating at an accelerating voltage of 5.00 kV and magnification of 1.00 kx.

The characterization of polyester fabrics was performed on electrokinetic analyser SurPASS, Anton Paar [10] through zeta potential (ZP, ζ). The zeta potential of standard, washed and aged fabrics was measured in the dependence of pH of electrolyte, 0.001 mol/l KCl, in the pH range from 10 to 2.

For determination of smoothness, softness, friction, compression, roughness and total active touch feel, the Fabric Touch Tester, FTT M293, SDL Atlas was used.

The thickness of the polyester fabric was determined in accordance with EN ISO 5084:2003-Textiles-Determination of thickness of textiles and textile products. Changes in the thickness (dh) of the fabric after ageing and 10 washing and cycles compared to the initial thickness were obtained according to equation 1 [11].

$$dh = (h1 - h2)/h2 \times 100\ (\%) \quad (1)$$

where is: h1-thickness of pristine fabric (mm); h2-thickness of aged or washed fabric (mm)

Whiteness quality of polyester fabrics was determined and evaluated by whiteness degree (W_{CIE}) on a remission spectrophotometer Datacolor 850, Switzerland.

The breaking force and elongation of the polyester fabrics was measured by the strip method in the warp direction according to EN ISO 13934-1:2013, using a Tensolab 3000 dynamometer, Mesdan s.p.A.

3. Results

In this paper, the influence of multiple washing and artificial ageing on the properties of standard polyester fabrics was researched.

For the characterisation of the fibre surface of polyester fabrics, scanning electron microscopy was used. SEM images showed the visible surface changes after washing, Fig. 3b. It can be seen characteristic accumulations of some deposits on the fibre surface, if compared to the standard and aged one, which is indicating the presence of detergent after the washing process, Fig. 3.

DOI: https://doi.org/10.26799/cp-gams2022

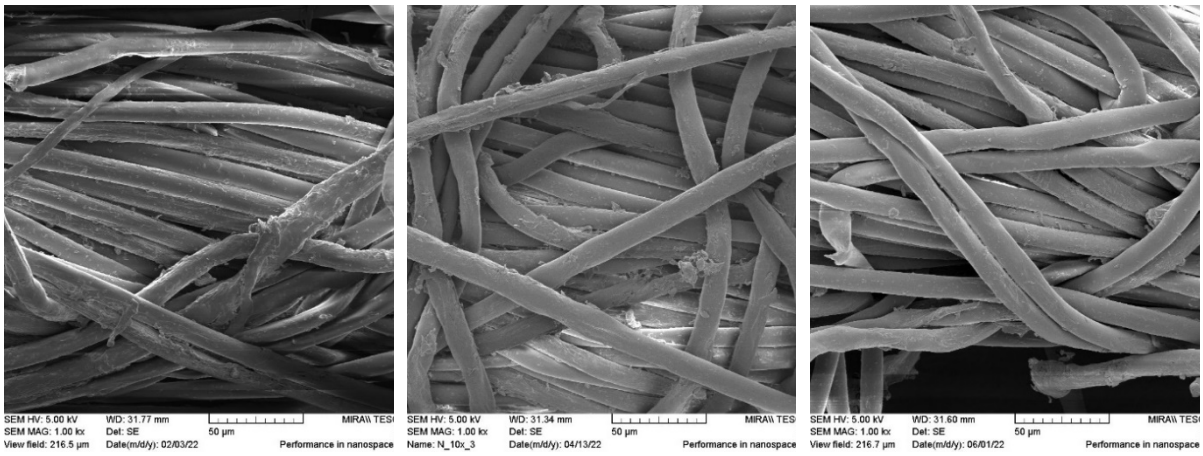

a.) b.) c.)

Fig. 3: SEM images of standard polyester fabric surface: a.) standard, b.) washed and c.) aged

The curve of zeta potential of the standard polyester fabric shows less negative value that is commonly for polyester fabric. The negative zeta potential of this sample in alkaline medium is around -18.0 mV, Fig. 4. Washed polyester fabric has more negative value (-25.0 mV), which indicates some surface modification happened. This modification is caused by washing conditions. Because of the alkali medium, the polyester is getting hydrolysed with more available negative –COOH groups [12,13]. The zeta potential of 75 hours aged polyester fabric, which corresponds to 750 h of natural sun exposure, has shown slightly positive value (-14.0 mV) than the zeta potential of the standard and washed polyester fabric.

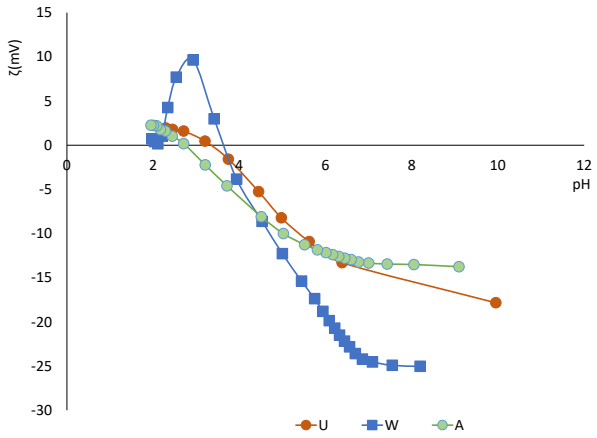

Fig. 4: Zeta potential of standard, washed and aged polyester fabric

Multivariate analysis (MVA) is used to analyse complex data sets and their relationships. That is a method that counts similar things that are close to each other in the same space for particle size distribution data of washing and ageing processes, Fig. 5 [14].

DOI: https://doi.org/10.26799/cp-gams2022

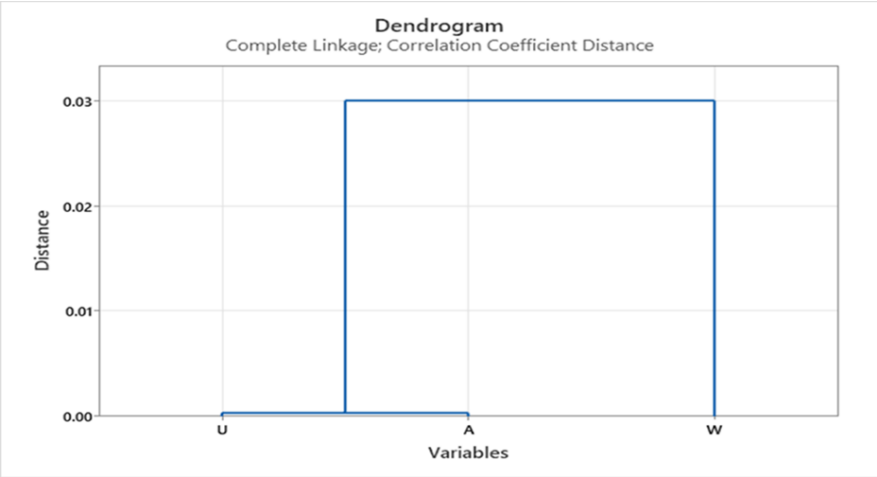

Fig. 5: Dendrogram of the MVA for the difference of polyester samples before and after washing and aging.

Small differences are observed in aged and washed samples and they are classified in the same group compared to the untreated sample.

Tab. 3: FTT primary hand and feel report

Fabric	Bending (N m /rad)	Compression CW(N m)	Friction	Smoothness	Softness	Warmth	Total Active Touch Feel
U	$1.23*10^{-3}$	$2.56*10^{-3}$	0.25	4.0	2.0	2.0	3.0
W	$1.94*10^{-3}$	$5.18*10^{-3}$	0.26	3.0	3.0	3.0	3.0
A	$1.13*10^{-3}$	$2.29*10^{-3}$	0.29	3.0	3.0	3.0	3.0

FTT is an instrument for measuring of primary textile comfort and is able to measure the objective assessment of fabric quality and performance with 18 indices through the measuring in warp and weft direction. On the basis of these indices, by this instrument can be predicted the primary sensory indices, PSI, so-called tactile properties of hand touch and feel: smoothness, softness, warmth, and total active touch feel. For active touch feel, standard polyester fabric, U, was quoted as slightly smoothness (grade 4) than W and A (grade 3), Tab. 3. Smoothness, softness and warmth of W and A fabrics are identical. The summary results of total active touch feel at the end showed the same results (grade 3) for all polyester fabrics (U, W and A).

Tab. 4: Fabric properties before and after exposure to washing and ageing

Fabric	Thickness (mm)	Change in fabric thickness dh (%)	Whiteness W_{CIE}	Breaking force F_B (N)	Elongation ε (%)
U	0.3540	-	49.95	689.5	23.167
W	0.4060	-0.15	52.87	397.0	13.615
A	0.3760	-0.06	31.97	658.0	19.935

From the Tab. 4 can be seen differences in the thickness of washed and aged polyester fabrics compared to the standard polyester fabric. It is evident the change in thickness of the washed and aged samples. Washed polyester fabric shows an increase in the fabric's thickness in the multiple washing process. The reason for such behaviour is shrinkage of the washed fabrics during washing. The lowest whiteness degree shows artificial aged polyester fabric, which is expected. Namely, it is well-known that UV rays cause yellowing of the white material. The results of breaking force indicate that the washing causes changes in mechanical properties, which are significantly decreased (from 689.5 N for standard, untreated fabric to 397.0 N after 10 washing cycles). The artificial ageing has only a minor impact on breaking force, a decrease of 31.5 N.

DOI: https://doi.org/10.26799/cp-gams2022

4. Conclusion

The evaluation of the surface properties of polyester fabrics after washing and artificial ageing was monitored. The results indicate some modification potential of ageing and washing:

- SEM images of aged and washed samples differed in smoothness; the surface of aged sample is smoother than washed one
- Zeta potential results revealed that ageing had a stabilising effect, whereas washing caused more negative values of polyester fabric due to hydrolyzing polyester fabric.
- MVA is an acceptable method for assessing and distinguishing polyester samples before and after light exposure and washing
- The results of total active touch feel showed the same grade 3 for all polyester fabrics, so it can be concluded that surface properties were not impaired

Acknowledgements

The work of doctoral student Ana Šaravanja has been supported in part by the "Young researchers ' career development project training of doctoral students", DOK-2021-02-6750, of the Croatian Science Foundation. This work has been supported in part by Croatian Science Foundation under the project IP-2020-02-7575, InWaShed MP.

References

1. N.L. Merlin and K. Balasubramanian, "Effect of microplastics in water and aquatic systems", *Environ. Sci. Pollut. Res*., vol. 28, pp. 19544–19562, 2021.
2. S. Kolbe, "Mikroplastika ili mikrovlakna?" *Tekstil*, vol. 67, no. 7-8, pp. 235-236, 2018.
3. I. Čorak et al, "Enzimi za hidrolizu poliestera", *Tekstil*, vol. 68, no. 7-9, pp. 142-151, 2019.
4. I. E. Napper, R.C. Thompson, "Release of synthetic microplastic plastic fibres from domestic washing machines: Effects of fabric type and washing conditions", *Mar. Pollut. Bull.*, vol. 112, no. 1-2, pp. 39-45, 2016.
5. M. Sillanpää and P. Sainio, "Release of polyester and cotton fibers from textiles in machine washings. Environ", *Sci. Pollut. Res,* vol. 24, no. 23, pp. 19313–19321, 2017.
6. E. Richaud and J. Verdu, "Aging behavior and modeling studies of unsaturated polyester resin and unsaturated polyester resin-based blends",in *Unsaturated Polyester Resins*, Elsevier, 2019, pp.199-231.
7. L. W. Hunter et al., "A materials aging problem in theory and practice", *Johns Hopkins APL Tech.Dig*. vol. 21, no. 4, pp. 575–581, 2000.
8. I. Salopek Čubrić et al "Behavior of Polymer Materials Exposed to Aging in the Swimming Pool: Focus on Properties That Assure Comfort and Durability", *Polymers*, vol. 13, no. 15, pp. 2414, 2021.
9. J.R. White, "Polymer ageing: Physics, chemistry or engineering", *Time to reflect. Comptes Rendus Chim*, vol. 9, no. 11-12, pp. 1396–1408, 2006.
10. Luxbacher, T. et al, "The zeta potential of textile fabrics: a review", *Tekstil*, vol.65, no. 9-10, pp. 346-351, 2016.
11. T. Pušić et al., "Electromagnetic Shielding Effectiveness of Woven Fabric with Integrated Conductive Threads after Washing with Liquid and Powder Detergents", *Polymers* vol. 14, no. 12, pp. 2445
12. Luxbacher, T., Pušić T. and Bukšek, H, "The zeta potential of textile fabrics: A review" Tekstil 2016, 65, 346–351.
13. Flinčec Grgac, S. et al., "The Chitosan Implementation into Cotton and Polyester/Cotton Blend Fabrics", *Materials* vol. 13, no 7, pp. 1616, 2020.
14. M. Čurlin et al"Particle Characterization of Washing Process Effluents by Laser Diffraction Technique, " *Materials*, vol. 14, no. 24, pp. 7781, 2021.

Proceedings of the GAMS 2022 International Conference
Paris, France – June 15 – 17, 2022
DOI: https://doi.org/10.26799/cp-gams2022

Zn-rich Coatings Dried with Infrared (IR) Radiation

Ivan Stojanović[1], Lovro Turkalj[1*], Ivan Cindrić[1*], Ivan Juraga[1], Marin Kurtela[1], Vinko Šimunović[1], Vesna Alar[1], Hrvoje Franjić[2]

[1] Faculty of Mechanical Engineering and Naval Architecture, University of Zagreb, Ivana Lučića 5, Zagreb, Croatia, lovro.turkalj@fsb.hr, ivan.cindric@fsb.hr
[2] Končar Steel Structures Inc., Fallerovo šetalište 22, Zagreb, Croatia, hrvoje.franjic@koncar-mk.hr

Abstract

Zinc-rich primers (ZRP) have unique property of metal protection even when there is a slight mechanical damage to the coating due to its cathodic protection mechanism. They are often used as primer coatings in various aggressive environments such as offshore, industrial, etc. For the successful protection, Zn-rich (Zn (R)) coatings need to be applied to clean surface, properly mixed and dried. There is an increasing tendency to find more efficient drying methods while maintaining the good coating protective properties due to the technical and economic factors. Infrared (IR) drying technology presents itself as one such method. The aim of this paper is to determine the influence of different IR drying parameters on Zn-rich coating protective efficiency and the drying speed. The observed parameters are the distance of the samples from the IR radiation source and the thickness of the mild steel plates. Pull-off test was done on the samples after drying to determine if the coatings were chemically crosslinked and ready for exploitation. Coating resistance was determined by electrochemical impedance spectroscopy (EIS) and corrosion properties were evaluated with accelerated corrosion tests. The results show increase in the drying time with the increase in the distance from the IR radiation source as well as the thickness of the samples. However, when comparing conventional drying methods and IR technologies, IR drying achieves significant savings in drying times with no negative effect on coating protective properties.

Keywords: zinc-rich primers, infrared drying, electrochemical impedance spectroscopy, corrosion

1. Introduction

One of the most practical and cost-effective ways to slow down or prevent corrosion is to apply an adequate protective coating. Coatings can be applied over large areas with relatively small layer thicknesses. The application process is quick, as the associated material and labour costs are usually much lower than the cost of the protected object. Over the last century, the technology of corrosion-resistant coatings has been constantly evolving, resulting in a wide range of products to protect different substrates in various conditions [1]. Zinc and its alloys have an essential role regarding the protection of other metals, in particular mild steel. They are the most common and widely used anode materials which provide galvanic protection of steel substrates, thus leading to the development of zinc-rich (Zn (R)) coatings [2]. Coating industry was highly affected with emerging requirements for reducing volatile organic compounds (VOC), which has led to the appearance of new coating systems and drying methods [3]. A particular direction in which the development of drying methods has led is infrared (IR) energy. IR energy is a type of radiation which belongs between the range of visible light and microwaves in the electromagnetic spectrum. The radiation generally speeds up the drying process of all coating types (Figure 1). IR drying of coatings also has a positive impact on the environment in terms of reducing energy consumption and VOC emission by 50% [2]. In this paper, solvent-based Zn (R) primer was applied on steel samples and dried by IR radiation and on atmospheric conditions. The aim of this paper is to determine how changes in the distance from the source of IR radiation and the thickness of steel samples affect drying times and the quality of the coating. Drying quality was evaluated by adhesion tests and visual inspection, as good adhesion is crucial for the integrity and longevity of the coated sample. Protective properties were assessed in a chloride environment using a salt spray chamber. Coating resistance was obtained by electrochemical impedance spectroscopy (EIS), while electrochemical potential state was determined by open circuit potential.

DOI: https://doi.org/10.26799/cp-gams2022

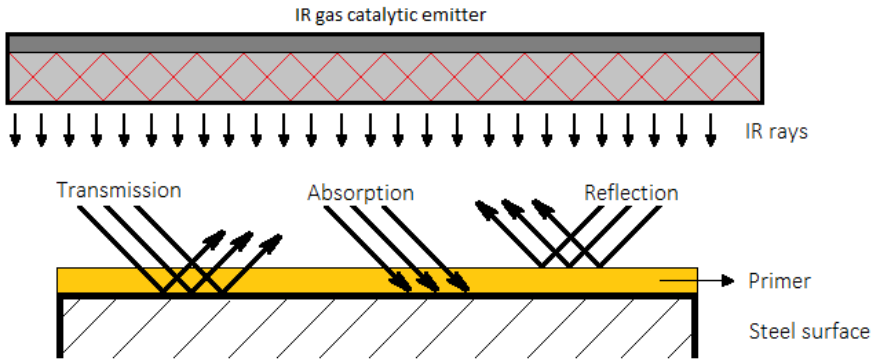

Figure 1. Primer curing process with IR emitter

2. Materials and methods

Two-component solvent-borne (SB) epoxy primer containing zinc was applied on various thicknesses of mild steel samples and cured at different drying distances from the IR emitter. Various changes in the distance from the IR source and sample thicknesses were observed to determine their affection on the drying times of the coating. Pull-off adhesion tests were carried out to resolve the crosslinking degree. All dry film thicknesses (DFTs) are in the range from 60 µm to 80 µm. An IR chamber based on catalytic infrared radiation (CIR) was used for to accelerate the drying process operating with wavelengths from 2 to 10 µm. Protective properties were evaluated in a chloride environment using a salt spray chamber. Electrochemical potential state was determined by open circuit potential (OCP) measurements, while coating resistance was obtained with electrochemical impedance spectroscopy (EIS).

3. Results and discussion

It can be evaluated that the drying time increases proportionally as the steel samples thickness grows and the drying distance increases (Figure 2). Comparing obtained drying time results with required air-drying time according to the coating technical specification sheet, IR technology significantly shortens the drying process by several hours. Most of the initial Pull-off test values display sufficient adhesion results according to ISO 12944-6 (Figure 3). A decrease in measured values can be noted as the distance from the IR radiation source increases. Following Pull-off tests (after 72h) indicate higher adhesion values which can be affirmed to progressive hardening of the coating.

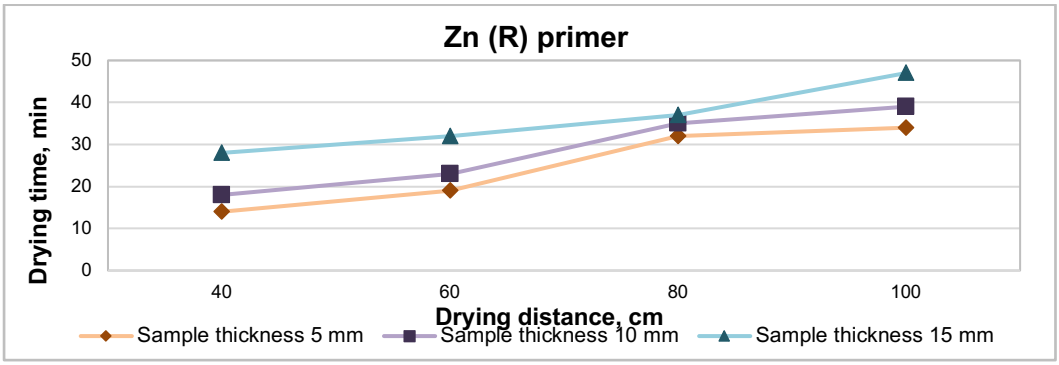

Figure 2. Drying times based on different steel sample thicknesses and distances from the IR radiation source

DOI: https://doi.org/10.26799/cp-gams2022

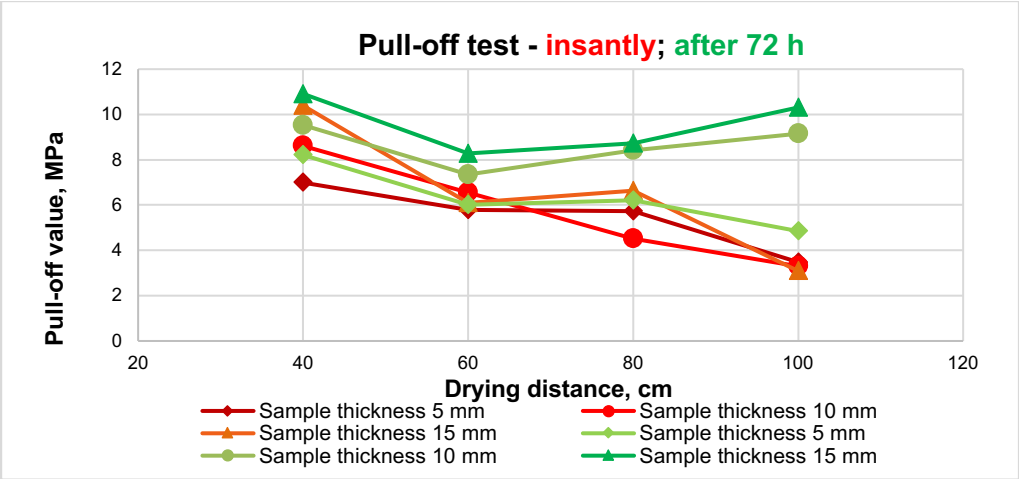

Figure 3. Drying times based on different steel sample thicknesses and distances from the IR radiation source

After 5 days (120 h) of accelerated corrosion test in the salt spray chamber (ISO 9227), coated samples did not show any signs of rusting, cracking, flaking and blistering, according to ISO 4628 (Figure 4). There was no spread of corrosion around the cut beside corrosion which appeared on the edges, which was not taken into consideration. Zinc corrosion products are visible after 5 days of accelerated corrosion test, which indicates its cathodic protection mechanism.

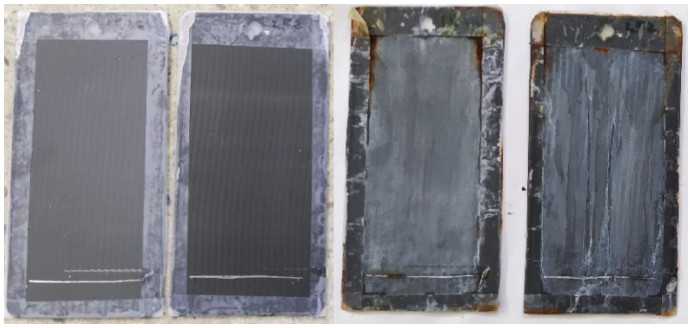

Figure 4. Test samples before (left) and after 5 days (right) of accelerated corrosion test

Electrochemical analyses were performed in 3,5% NaCl solution. After 5 days, OCP results indicated stable corrosion potential over time which indicates great protective properties of the coating. EIS plots were fitted to a certain model which notes to very good barrier properties. Resistance value was up to the 10^8 Ω after 24 h, with increase in resistance after 5 days which indicates an effect of zinc particles and their cathodic protection mechanism (Figure 5).

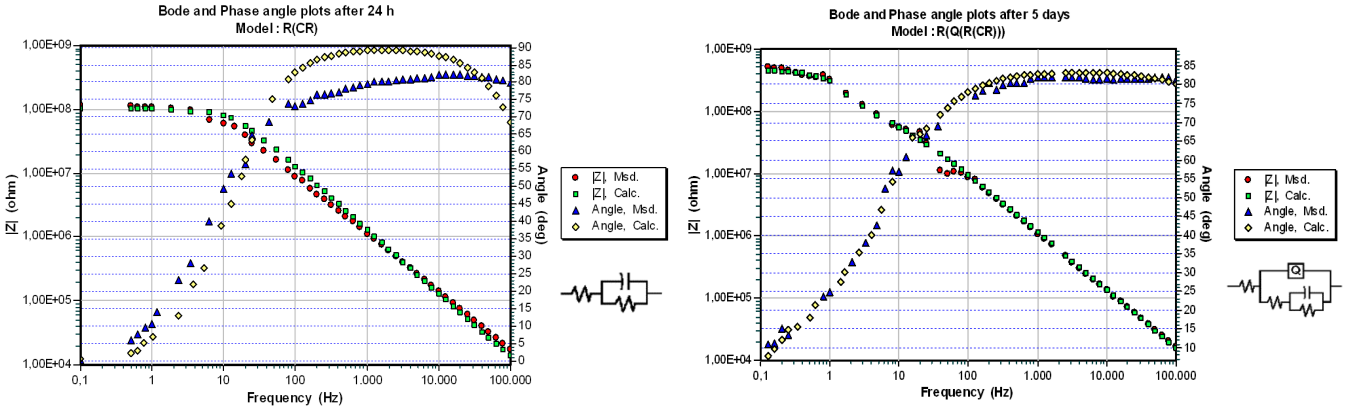

Figure 5. Bode and Phase angle plots after 24h (left) and 120 h (right) in 3,5 % NaCl solution

DOI: https://doi.org/10.26799/cp-gams2022

4. Conclusion

To mitigate corrosion on steel surfaces, zinc-rich primers (ZRP) are considered to be one of the best coating options used in hazardous environmental conditions. To accelerate the entire coating application process, catalytic IR technology was used. Study results generally indicate significantly shorter drying times of liquid coatings with IR technology. The observed parameters were different thickness steel substrates protected by epoxy primer coating which were dried at various distances. Despite the fact of reduced drying times in comparison with air cured ones, it was observed that drying times strongly depends on the sample thickness and the distance from the IR emitter. With the increase of the sample thickness and the distance from the IR source, the drying time increases. Adhesion results point out the subsequent hardening of the coating throughout the period of 72 hours at room temperature, which can be avoided with prolonged drying times. Accelerated corrosion tests in salt spray chamber were satisfactory which implies that IR radiation does not have a harmful influence on the coating anticorrosive properties. Electrochemical analyses showed very good protective properties of the coating, due to the cathodic protection from zinc particles. From all of the results above, catalytic IR technology proved to be a good and reliable way to accelerate the process of corrosion protection for mild steel structures and products with no negative effect on the coating protection quality.

Acknowledgements

This study is part of the project “Smart plant for drying liquid coatings” which is co-financed within the Operational Programme Competitiveness and Cohesion from the European Regional Development Fund under reference number KK.01.2.1.02.0030. The content of the published materials is the sole responsibility of the Faculty of Mechanical Engineering and Naval Architecture.

References

1. Hang T. T. X., Truc T. A., Nam T. H., Oanh V. K., Jorcin J. B., Pébère N. (2007). Corrosion protection of carbon steel by an epoxy resin containing organically modified clay, Surface and Coatings Technology, pp. 7408-7415, Volume 201. https://doi.org/10.1016/j.surfcoat.2007.02.009
2. Stojanović, I. Cindrić, I. Janković, L. Šimunović, V. Franjić, H. (2022). Performance Assessment of Differently Dried Coating Systems for Potential Application in the Power Transformer Industry, Coatings 2022, 12, 331. https://doi.org/10.3390/coatings12030331
3. Buchheit R.G. Handbook of Environmental Degradation of Materials, 3rd Edition, pp. 449-468, 2018., Elsevier